Semi-global symplectic invariants of the Euler top

by

George Papadopoulos

A thesis submitted to the
Faculty of Science
University of Sydney
in partial fulfilment of the
requirements for the degree of
Master of Science

School of Mathematics and Statistics

Sydney, New South Wales, Australia

May 2013

Abstract

The semi-global symplectic invariants were introduced by Dufour et. al. as a means of verifying equivalence of integrable systems in one degree of freedom. In the main part of the thesis we explicitly compute the semi-global symplectic invariants near the hyperbolic equilibrium point of the Euler top, otherwise known as the rigid body. As an interim step, the Birkhoff normal form of the Hamiltonian at this point is computed using Lie series. The Picard-Fuchs ODE for the action near the hyperbolic equilibrium is derived. Using the method of Frobenius on the Picard-Fuchs equation we show that the Birkhoff normal form can also be found by inverting the Frobenius series of the regular action integral. Composition of the regular action integral with the singular action integral leads to the symplectic invariant. To our knowledge this is the first time that such invariants near a hyperbolic point have been computed explicitly using the Picard-Fuchs equation. Finally we discuss the convergence of these invariants using both analytical and numerical arguments, as well as explore the possibility of equivalence with the pendulum.

Contents

Preface

This thesis is based upon the present 2012 work by Papadopoulos and Dullin in [25]; it presents the first time that the semi-global symplectic invariants of the Euler top near the hyperbolic equilibrium have been explicitly calculated. This thesis contains the contents of that paper, along with more background discussion and additional detail in some calculations.

In the first part of the thesis we first provide an introduction, background theory and literature supplementing the mathematical results and calculations in the second part. This includes citing classical contributions by Euler himself, derivations of some fundamental results from graduate level mathematical mechanics, physical real-world motivations and analogies, and a chronological review of the literature. The second part of the thesis contains the main calculations and results. The Birkhoff normal form of the Hamiltonian is found via the method of Lie series. The Picard-Fuchs ODE, with solutions being the actions, is derived and the method of Frobenius is used to produce series expansions of the actions. We find that the Birkhoff normal form can be found by inverting the series representation of the regular action integral.

The main result of the current research is presented in this thesis, namely the semi-global symplectic invariants of the Euler top are explicitly calculated. The symplectic invariant is given by the regular part of the action integral near a separatrix written in a canonical coordinate system defined using the Birkhoff normal form at the hyperbolic equilibrium point. Theorem 1.3 states that we can use these invariants to determine if two integrable systems are equivalent; this theorem motivates us to calculate the semi-global symplectic invariants of the Euler top. This is the first step that may lead

to a non-trivial equivalence between the Euler top and other Hamiltonian systems with one degree of freedom. We can, for example, decide whether a particular Euler top (it is a three parameter family) is equivalent to say the pendulum, for which the invariants have been calculated in [9].

We find that both the Birkhoff normal form and the symplectic invariant series converge; this is discussed using both analytic and numerical arguments. The end of the thesis concludes with the uses and applications of the invariants of the Euler top. We find that the pendulum is *not* equivalent to a particular Euler top, and that in future work it may be possible to find how the symplectic invariants dictate the tumbling phenomenon observed during an unstable rotation.

Chapter 1

Introduction

The *Euler top* is a classical *Hamiltonian* system which describes the rotational motion of a *rigid body* in *free space* in the absence of a potential. The word "rigid" here refers to the assumption that during the motion, the distance between any two particles always remains constant. Note that this assumption is valid for a system or continuum of particles; the latter is most commonly associated with the term "rigid body". The motion is studied in a *non-inertial* co-ordinate system that is stationary relative to (and has its origin located at) the *centre of mass* of the rigid body. Note that sometimes we call this the *centre of mass frame* or the *body frame*. Since this frame is stationary relative to the centre of mass, translations and forces are non-existent. In the centre of mass frame this can be considered as the rotation of the rigid body about a fixed point. The origin is not always chosen to be the centre of mass of the body frame, if convenience dictates otherwise; such an example is the analysis of the *heavy top*. Although we have specified that the dynamics is "in the absence of a potential", we do not mean to say that the top cannot be in a potential. To be more specific, this means that relative to the body frame, the dynamics of the top is equivalent to a *potential-free space*. Such an example is the gravitational potential; it is known from basic mechanics that the physics taking place within a free-falling frame on Earth is equivalent to a frame in space far removed from any gravitational fields. The top is "free" in the sense that there are no components of frictional,

electromagnetic or any other forces that may cause an effect which is visible relative to the body frame. Thus in the body frame there must be no net torques acting on the top.

This system has been treated extensively in the literature for the last 300 years. Classical rigorous treatment began with Leonhard Euler in the mid-18th century, whereby the system now bears his name. A couple of notable contributions are [12, 13]. From there, the rigid body became a tenet of mathematical physics, and was the standard foundation upon which more involved mechanics was constructed and taught. It features in many chapters of modern standard graduate mechanics texts, including [1, 16, 17, 18, 19, 27].

1.1 Physical applications and motivations for study

Before diving into the mathematics behind this work, we will present a few common physical examples of rotations. It should be noted however, that none of the examples in this section will be analysed in the main part of the thesis. However, we believe that the results that arise from the reduced problem in this work, may be able to be extended and/or applied to more complex dynamics such as those presented here, and as such could be a source for future research continuing on from the results of this work. In particular, the following examples often conjure up curiosity and popularity amongst even the general public, and often prove to be a good starting point for discussion of motivation for this field of research.

Other than the numerous applications to inanimate objects such as celestial bodies, sports equipment and aircraft, there are also anatomical applications to the bodies of living creatures. Whilst these are certainly not rigid, they can be defined as *piecewise-rigid* bodies. However the dynamics governing them is non-linear and often chaotic. As an example, consider the change in complexity between the ordinary pendulum which is rigid, and the double pendulum which has two rigid pieces. Such bodies cannot be completely analysed analytically, so must be numerically analysed (we will not

be studying any such bodies, but simply state it here for interest).

[27] gives two particularly interesting creatures that are studied, the cat and the human being. There is a common experiment whereby a cat is dropped from a safe height from various initial linear and angular positions and velocities. We observe that, after the struggle to free itself, the cat always manages to land safely on its feet. Even for those who have not studied physics, there is a sense of paradox here; there is an apparent violation of the *conservation of angular momentum*. What does the cat do to change its orientation mid-air? Is it the way it pushes itself off from where it is released? A similar situation to this is diving. Here, we watch and marvel at how divers can apparently merely push themselves off a diving platform in one direction, only to tumble through the air in nearly all possible orientations and directions. Even a physics student may ask, "How is it that the diver simply pushes forward, giving one initial angular momentum, to end up twisting sideways, which apparently gives the diver a completely different angular momentum? Is it the way the diver pushes off the diving platform? Or the formation of the arms and legs mid-dive?"

Careful analysis of the mathematics and physics involved leads us to conclude that neither the cat nor the diver perform black magic, and that angular momentum is conserved, as always. In particular, the falling cat phenomenon is a consequence of the fact that the cat is not a rigid body, but instead deforms its shape in mid-flight. This is presented in [21], where they use the gauge theory for deformable bodies. In this work, the Euler top is not a deformable body so these types of rotations will not be studied or presented here.

In this thesis, we will be studying rigid bodies, so we present a more suitable experiment that will directly relate to the Euler top. It should be noted however that the following example requires a description of the full 3-dimensional dynamics in $SO(3)$, whereas later on we will be reducing our dynamics to 1D. Even so, it is a useful introduction to the exploration of the phenomenon yielded by unstable rotations of rigid bodies, which is the main focus of this work.

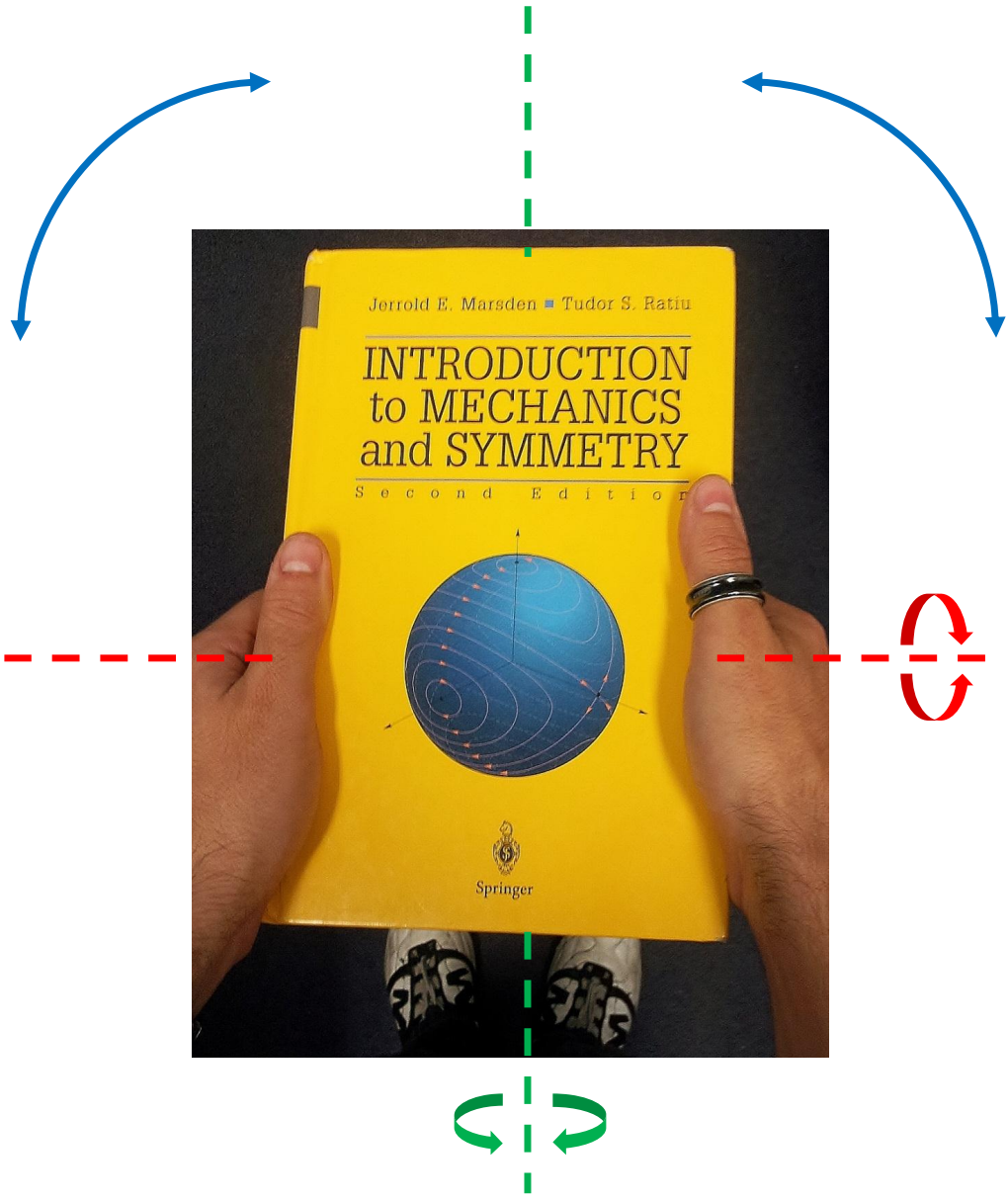

Figure 1.1: A book showing three distinct principal moments of inertia as an example of a simple Euler top.

Consider holding a book (or any rigid object in the shape of a rectangular prism with no square cross-sections), as illustrated in Figure 1.1. There are three "natural" ways in which to flip the book, which are the principal axes of rotation. Namely, about the two dashed axes in red and green, and an axis perpendicular to both of these (indicated the rotational curved arrows in blue). The aim is to flip the book and perform one full rotation about that axis so as to catch it when it arrives back to the original configuration; that is the front cover with text in a legible upright orientation. One finds that this is easily done about two non-horizontal axes (relative to the book) in blue and green. But strange things start to happen when one tries the same about the horizontal dashed axis in red. The reader will not be able to tumble the book neatly, no matter how hard they try. In attempting to catch the book, the reader finds they can catch it in two orientations that should not be possible. If it is caught *early*, the reader views the back cover showing with the text legible (that is the right way up). If it is caught *late*, the front cover is viewed with the text illegible (that is upside down). To get to either of these configurations, the book must undergo two half-rotations about *two* of the axes of rotation. Even then, the book is not in its original configuration. How could this be so? If an initial angular velocity was imparted upon the book about the horizontal axis only, where did the torque come from needed to turn it about another axis? The answer lies in the fact that the rotation about the horizontal axis is *unstable*, whereas the other two rotations are *stable*. This is a consequence of the *Rigid Body Stability Theorem* on page 16, which we will come across in the next section. That means, that if one were able to *perfectly* supply an initial torque along the unstable axis, a perfect rotation would result. However, a small perturbation in the rotation about the unstable axis causes the rotation to deviate towards this uneven tumbling motion that appears as two half-rotations about two axes.

We find that we have asked similar questions before, in the case of the tumbling cat and diver. So answering these questions in the case of rigid bodies like the book is the first step in understanding the tumbling of nat-

ural bodies, both rigid like spacecraft and piecewise-rigid like the anatomies of living beings. In fact, [27] goes on to conclude that "there is no doubt that finite reorientation is consistent with conservation of angular momentum", using an astronaut as an interesting example of a piecewise-rigid body with elementary but convincing physical arguments. However, these are more complicated phenomena that cannot be fully explained by just considering the reduced one degree of freedom motion. Instead one actually has to consider the rotational motion, namely the dynamics on $SO(3)$ driven by the solution of the dynamics in the body frame. We believe though, that insight into the details of the hyperbolic dynamics of the reduced Euler top may help to better understand the tumbling book phenomenon in a future research project.

1.2 Mathematical framework

We proceed to define the Euler angles in a similar fashion to [27]. In general, rotations in three dimensions (that is, elements of $SO(3)$) do not commute. Thus, the rotations must be taken one at a time, which causes the co-ordinate axes to change. Let us consider a frame (x, y, z) who's origin is the body's centre of mass. After each rotation we arrive at a new set of axes. In particular, starting with the "spacial frame" (x, y, z), we rotate about the z-axis by an angle ϕ to arrive at new axes (x', y', z'). Then we rotate about the x'-axis by an angle θ to obtain axes (x'', y'', z''). Finally, rotate about the z''-axis by an angle ψ to obtain the final body frame (x''', y''', z'''). Thus, defining $\mathcal{R}_{\text{axis}}(\text{angle})$ as the rotation about a particular axis by a particular angle, we have

$$(x, y, z) \overset{\mathcal{R}_z(\phi)}{\longmapsto} (x', y', z') \overset{\mathcal{R}_{x'}(\theta)}{\longmapsto} (x'', y'', z'') \overset{\mathcal{R}_{z''}(\psi)}{\longmapsto} (x''', y''', z''')$$

and so the position or orientation of the Euler top can be completely determined by the variables (ϕ, θ, ψ). We further clarify the notion of "absence of potential"; we can consider the motion in any potential (such as gravity) that does not depend upon the Euler angles. Finally we find that the angu-

lar velocity vector $\mathbf{\Omega}$ in the body frame can be written in terms of the time derivatives of the Euler angles, namely

$$\mathbf{\Omega} = \begin{pmatrix} \Omega_1 \\ \Omega_2 \\ \Omega_3 \end{pmatrix} = \begin{pmatrix} \sin\psi\,\dot{\theta} \\ \cos\psi\,\dot{\theta} + \sin\theta\sin\psi\,\dot{\phi} \\ \dot{\psi} + \cos\theta\,\dot{\phi} \end{pmatrix}.$$

We now proceed to consider the rotation matrices $\mathcal{R}$ in a similar fashion to [16]. Consider a fixed point on the body. We denote this point by $\mathbf{X}$ in the body frame, and $\mathbf{x}(t)$ in the spacial frame. Clearly $\mathbf{X}$ can also be interpreted as an initial point on the top as measured in the spacial frame, and would be denoted by $\mathbf{x}(0)$. We now change our notation slightly to show an explicit dependence on the rotation on time, namely $\mathcal{R}(t)$. Then the position in the spacial frame at some time t depends upon the initial configuration of the body, namely

$$\mathbf{x}(t) = \mathcal{R}(t)\mathbf{X}.$$

Differentiating this yields the differential equation

$$\dot{\mathbf{x}} = \dot{\mathcal{R}}\mathcal{R}^{-1}\mathbf{x}.$$

Thus in this way, we can think of $\mathcal{R} \in SO(3)$ as a map from the body frame to the spacial frame. The angular velocity vector $\boldsymbol{\omega}(t)$ in the spacial frame is defined via

$$\dot{\mathbf{x}} = \boldsymbol{\omega} \times \mathbf{x}.$$

We can convert it to the body frame via

$$\mathbf{\Omega} = \mathcal{R}^{-1}\boldsymbol{\omega}.$$

The body angular momentum $\boldsymbol{L} := (L_1, L_2, L_3)$ and body angular velocity are related to each other from classical mechanics. We define the *moment of inertia tensor* M, where

$$\boldsymbol{L} = M\mathbf{\Omega},$$

which is a symmetric positive-definite matrix that can be diagonalised. Thus

we are free to choose how to align our axes, so we may as well choose them in such a way that M becomes diagonal, that is assume

$$M = \operatorname{diag}(\Theta_1, \Theta_2, \Theta_3),$$

whose elements are called the *principal moments of inertia.*

In our work (without loss of generality), we shall assume the ordering

$$0 < \Theta_1 < \Theta_2 < \Theta_3. \tag{1.1}$$

Furthermore, from mechanics we have the following Theorem.

Theorem 1.1 (Perpendicular Axis Theorem)**.** *The principal moments of inertia satisfy triangle inequalities*

$$\Theta_i \leq \Theta_j + \Theta_k \tag{1.2}$$

for distinct $i, j, k \in \{1, 2, 3\}$, with equality occurring for planar bodies only.

We exclude the (degenerate) cases $\Theta_1 = \Theta_2$, $\Theta_2 = \Theta_3$, since in those cases there is no hyperbolic equilibrium. The special axes which make M diagonal are called the *principal axes*, which are orthogonal. In fact it was Euler in 1765 in [13] who first proved that every body has at least one set of three orthogonal principal axes.

In what follows, we use the following notational conventions. Letters written with tildes and sans-serif font denote unscaled and unshifted quantities respectively. In the absence of a potential, the *Hamiltonian* $\tilde{\mathsf{H}}$ is the rotational kinetic energy, and can be written as

$$\tilde{\mathsf{H}}(\boldsymbol{L}) = \frac{1}{2}\boldsymbol{L}^\top M^{-1}\boldsymbol{L} = \frac{1}{2}\sum_{i=1}^{3}\frac{L_i^2}{\Theta_i}. \tag{1.3}$$

Differentiating (1.3) yields

$$\boldsymbol{\nabla}\tilde{\mathsf{H}} = M^{-1}\boldsymbol{L}. \tag{1.4}$$

This way of writing the Hamiltonian is not symplectic as the angular mo-

menta are not canonical variables, but rather this system has a *Poisson structure*. Consider the *Poisson bracket* defined by

$$\{f, g\} := \boldsymbol{\nabla} f \cdot (P \boldsymbol{\nabla} g) \tag{1.5}$$

on the *phase space* P and real scalar functions $f, g : \mathrm{P} \to \mathbb{R}$. Then P is called the *Poisson structure matrix*. It can be shown that *Hamilton's equations* for a Hamiltonian H can be written succinctly as

$$\dot{\boldsymbol{x}} = P \boldsymbol{\nabla} H.$$

Canonical variables in n *degrees of freedom* are n pairings of *positions* with *conjugate momenta* of the form $\boldsymbol{x} := (\boldsymbol{x}_i)_{i=1}^{n}, \boldsymbol{x}_i := (q_i, p_i)$. Later we will see that the Euler top can be reduced down to one degree of freedom, whereby we simply have $n = 1 \Rightarrow \boldsymbol{x} = (q, p)$. In these variables, Hamilton's equations become

$$\dot{\boldsymbol{x}} = S \boldsymbol{\nabla} H,$$

where S is the *symplectic structure matrix* which is $2n \times 2n$ block diagonal with n diagonal entries

$$\begin{pmatrix} 0 & 1 \\ -1 & 0 \end{pmatrix},$$

which is the symplectic structure matrix for $n = 1$ degree of freedom. Thus if $P = S$ in (1.5) then we say the Poisson bracket is canonical, that is the system has symplectic structure.

The task now is to find the Poisson structure matrix of the Euler top described by the Hamiltonian in (1.3). [16, 19] draw some remarkable and beautiful relationships, two of them being

$$\begin{aligned} \hat{\Omega} &= \mathcal{R}^{-1} \dot{\mathcal{R}}, \\ \hat{\omega} &= \dot{\mathcal{R}} \mathcal{R}^{-1}, \end{aligned} \tag{1.6}$$

where we define the *hat map* in $\mathbb{R}^3$ via

$$\hat{\mathrm{u}} := \begin{pmatrix} 0 & -\mathrm{u}_3 & \mathrm{u}_2 \\ \mathrm{u}_3 & 0 & -\mathrm{u}_1 \\ -\mathrm{u}_2 & \mathrm{u}_1 & 0 \end{pmatrix}, \text{ where } \mathbf{u} := (\mathrm{u}_1, \mathrm{u}_2, \mathrm{u}_3).$$

The hat map is matrix left-multiplication equivalent of the cross product, that is $\hat{\mathrm{u}}\mathbf{v} = \mathbf{u} \times \mathbf{v}$. We can now see the fundamental role that the rotation matrix function $\mathcal{R}$ plays in determining the position in the spacial frame $\mathbf{x}$ as well as the angular momenta. From here we can construct a similar hat matrix from the body angular momentum vector

$$\hat{L} = \begin{pmatrix} 0 & -L_3 & L_2 \\ L_3 & 0 & -L_1 \\ -L_2 & L_1 & 0 \end{pmatrix}.$$

Define the *spatial angular momentum* as $\boldsymbol{l} := \mathcal{R}\boldsymbol{L}$. From here we can derive the famous *Euler equations* of motion of the Euler top. Differentiating yields

$$\begin{aligned} \dot{\boldsymbol{l}} &= (\dot{\mathcal{R}}\boldsymbol{L}) \\ &= \dot{\mathcal{R}}\boldsymbol{L} + \mathcal{R}\dot{\boldsymbol{L}} \\ &= \hat{\omega}\mathcal{R}\boldsymbol{L} + \mathcal{R}\dot{\boldsymbol{L}} \\ &= \boldsymbol{\omega} \times (\mathcal{R}\boldsymbol{L}) + \mathcal{R}\dot{\boldsymbol{L}} \\ &= (\mathcal{R}\boldsymbol{\Omega}) \times (\mathcal{R}\boldsymbol{L}) + \mathcal{R}\dot{\boldsymbol{L}} \\ &= \mathcal{R}\left((\boldsymbol{\Omega} \times \boldsymbol{L}) + \dot{\boldsymbol{L}}\right) \\ \Rightarrow \dot{\boldsymbol{l}} &= \mathcal{R}\left(\left(M^{-1}\boldsymbol{L}\right) \times \boldsymbol{L} + \dot{\boldsymbol{L}}\right). \end{aligned} \tag{1.7}$$

Equation (1.7) appeared in Euler's famous 1752 paper [12]. This paper was the defining groundwork for all future rigid body motion analysis up to the present day. In fact, it is in this paper that we see the first use of Newton's famous second law equation $F = ma$ in a more general setting using volume differentials. In the special case where there is no net torque acting on the

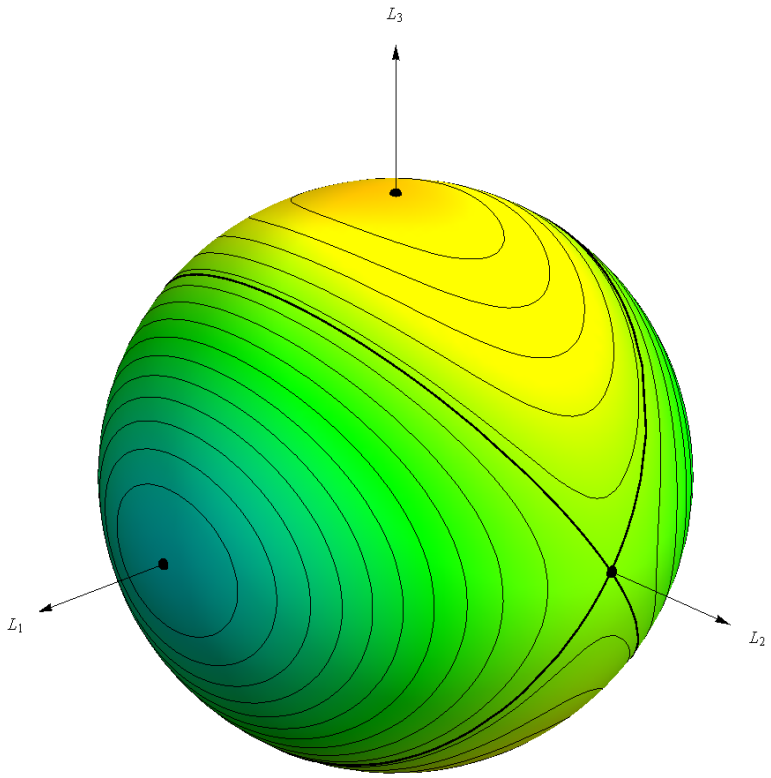

Figure 1.2: The phase space of the Euler top on $\mathcal{C}_\ell$.

top (as is the case with the Euler top), by conservation of angular momentum we have $\dot{\boldsymbol{l}} = \mathbf{0}$ and so

$$\dot{\boldsymbol{L}} = \boldsymbol{L} \times \left(M^{-1}\boldsymbol{L}\right) \tag{1.8a}$$

$$\Leftrightarrow M\dot{\boldsymbol{\Omega}} = (M\boldsymbol{\Omega}) \times \boldsymbol{\Omega}. \tag{1.8b}$$

Remark 1.1. The relation between $\hat{\Omega}$ and the rotation matrix $\mathcal{R}$ in (1.6) can be read as an ODE for $\dot{\mathcal{R}}$, once $\boldsymbol{\Omega}$ is known; this will give the actual rotation. Then the purpose of finding the symplectic invariants is to help describe $\boldsymbol{\Omega}$ and $\boldsymbol{L}$ near the separatrix.

Combining (1.8a) with (1.4) we see that $\hat{L}$ is exactly the Poisson structure matrix for the Euler top, since Hamilton's equations of motion for the Euler

top can be written as

$$\dot{\boldsymbol{L}} = \boldsymbol{L} \times \boldsymbol{\nabla}\tilde{\mathsf{H}} = \hat{L}\boldsymbol{\nabla}\tilde{\mathsf{H}}. \tag{1.9}$$

Due to conservation of angular momentum, the dynamics of the Euler top takes place on spheres of constant magnitude of angular momentum $\|\boldsymbol{L}\| = \ell$. Define a *Casimir function* C to be one which satisfies $\{C, F\} = \{F, C\} = 0$ for all functions F. Then we find that the total angular momentum is a Casimir $C(\boldsymbol{L}) := \|\boldsymbol{L}\|^2$ of the Poisson structure $\hat{L}$. The level set of the Casimir

$$\mathcal{C}_\ell \;:=\; \left\{\boldsymbol{L} \in \mathbb{R}^3 \colon C(\boldsymbol{L}) = \ell^2\right\}$$

is a sphere and the level set of the Hamiltonian, the *energy surface*

$$\mathcal{E}_{\tilde{\mathsf{h}}} \;:=\; \left\{\boldsymbol{L} \in \mathbb{R}^3 \colon \tilde{\mathsf{H}}(\boldsymbol{L}) = \tilde{\mathsf{h}}\right\}$$

is an ellipsoid with distinct semi-axes. The solution curves are given by the intersection $\mathcal{C}_\ell \cap \mathcal{E}_{\tilde{\mathsf{h}}}$ where we consider ℓ as fixed and $\tilde{\mathsf{h}}$ as varying. The (non-degenerate) intersections of the sphere with the ellipsoid give concentric ellipse-like curves, centred about elliptic equilibria of which there are four. There are two separatrices (which are great circles), the intersections of which occur at the two hyperbolic equilibria. In total there are six equilibria given by the degenerate intersections of the sphere with the ellipsoid, namely $\pm\ell\hat{\boldsymbol{L}}_i$, $i \in \{1, 2, 3\}$ where $\hat{\boldsymbol{L}}_i$ is defined as the unit vector along the L_i-axis. The following Theorem is quoted in [19] and states the stabilities of the equilibria.

Theorem 1.2 (Rigid Body Stability Theorem)**.** *In the motion of the Euler top, rotations about the largest and smallest principal axes are Liapunov stable, whilst rotation about the middle axis is unstable.*

Note. Ensure that $\hat{\boldsymbol{L}}$ is not confused with $\hat{L}$. The former is in bold-type to denote that it is a vector. The latter is not in bold-type to denote that it is a matrix.

We are interested in the unstable hyperbolic equilibria ($i = 2$), corres-

ponding to a rotation about the principal axis of inertia associated with the middle moment of inertia Θ_2. Figure 1.2 shows its location in phase space. The positive equilibria are shown as bold black points. The thinner contours are the intersections with $\mathcal{E}_{\tilde{\mathsf{h}}}$ which are the phase trajectories. The two thick contours are the separatrices. The positive hyperbolic equilibrium point located at $\ell\hat{\boldsymbol{L}}_2$ is clearly shown at the intersection of the separatrices. The other two positive points shown are stable elliptic type equilibria.

The linearisation of (1.9) at the hyperbolic equilibria is found by calculating the Jacobian, that is

$$D\left(\hat{L}\boldsymbol{\nabla}\tilde{\mathsf{H}}\right) = \begin{pmatrix} 0 & L_3\left(\frac{1}{\Theta_1}-\frac{1}{\Theta_3}\right) & L_2\left(\frac{1}{\Theta_2}-\frac{1}{\Theta_1}\right) \\ L_3\left(\frac{1}{\Theta_3}-\frac{1}{\Theta_2}\right) & 0 & L_1\left(\frac{1}{\Theta_2}-\frac{1}{\Theta_1}\right) \\ L_2\left(\frac{1}{\Theta_3}-\frac{1}{\Theta_2}\right) & L_1\left(\frac{1}{\Theta_1}-\frac{1}{\Theta_3}\right) & 0 \end{pmatrix}.$$

Evaluating at the hyperbolic equilibria gives

$$D\left(\hat{L}\boldsymbol{\nabla}\tilde{\mathsf{H}}\right)\Big|_{\boldsymbol{L}=\pm\ell\hat{\boldsymbol{L}}_2} = \frac{\mp\ell}{\Theta_2}\begin{pmatrix} 0 & 0 & \frac{\Theta_2-\Theta_1}{\Theta_1} \\ 0 & 0 & 0 \\ \frac{\Theta_3-\Theta_2}{\Theta_3} & 0 & 0 \end{pmatrix}$$

which has real eigenvalues $0, \pm\lambda$, where

$$\lambda = \frac{\ell}{\Theta_2}\sqrt{\frac{(\Theta_2-\Theta_1)(\Theta_3-\Theta_2)}{\Theta_1\Theta_3}}. \tag{1.10}$$

1.3 An introduction to symplectic invariants

In this section we introduce the theory behind the symplectic invariants. At first, we introduce an elementary geometric construction which leads to an interpretation of the symplectic invariants. After describing symplectic geometry in more detail, we introduce notions of equivalence between systems using the semi-global symplectic invariants. Finally, we give a brief chronological review of the literature in this field of study.

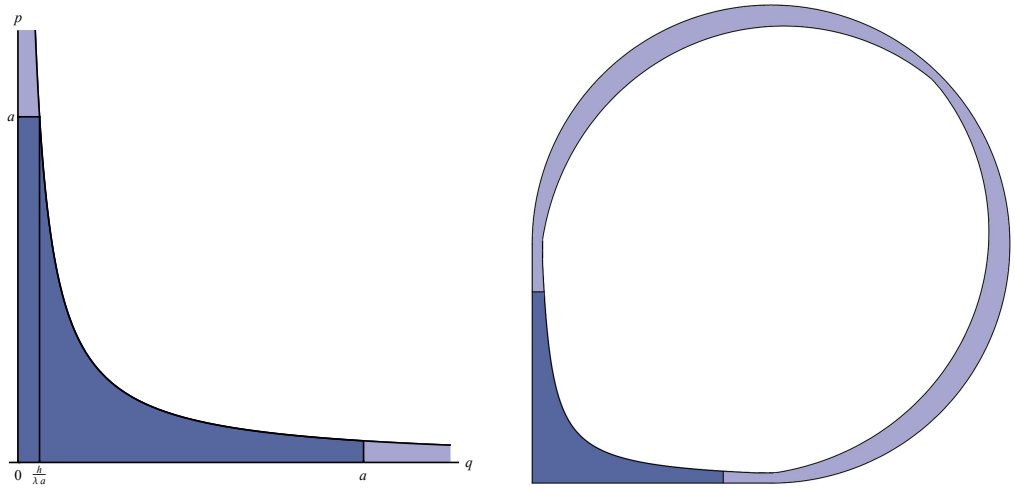

(a) A local picture of the symplectic invariant near the hyperbolic equilibrium point.

(b) A more global picture of the symplectic invariant near the separatrices.

Figure 1.3: Illustration of the geometric connection between the area bounded by the phase-plane curve and the separatrices and the symplectic invariant. Here we have canonical co-ordinates (q, p), the hyperbolic equilibrium point at the origin and the separatrices along the axes after a symplectic transformation.

1.3.1 Geometric connections

Consider a quadratic Hamiltonian H with value h and eigenvalue λ with a hyperbolic equilibrium point at the origin (whereby for simplicity, we have dropped any notational conventions momentarily). Then after a *symplectic* (area preserving) *scaling* and rotation of co-ordinates, the solution curve in canonical co-ordinate space (q, p) (as explained in Section 2.2) is the rectangular hyperbola $h = \lambda qp =: \lambda J$.

Consider calculating the area bounded by the hyperbola $h = \lambda qp = \lambda J > 0$, the separatrices $q, p = 0$ and the lines $q, p = a > 0$ for the first quadrant, namely the dark blue area as shown in Figure 1.3. We calculate the area under the curve $p = \frac{h}{\lambda q}$ over $\left(\frac{h}{\lambda a}, a\right)$, then add the area of the rectangular

region $\left[0, \frac{h}{\lambda a}\right] \times [0, a]$ to obtain

$$\begin{aligned}
\text{Area} &= \frac{h}{\lambda a} \times a + \int_{\frac{h}{\lambda a}}^{a} \frac{h}{\lambda q}\, \mathrm{d}q \\
&= \frac{h}{\lambda} + \frac{h}{\lambda} \left[\ln q\right]_{\frac{h}{\lambda a}}^{a} \\
&= \frac{h}{\lambda} + \frac{h}{\lambda} \ln\left(\frac{\lambda a^2}{h}\right) \\
&= J - J \ln J + 2J \ln a \\
&\sim J - J \ln J.
\end{aligned}$$

The calculation for the area corresponding to negative Hamiltonian is similar to what we present here. This area is not differentiable in the limit as $J \to 0$. The *symplectic invariant* σ can be thought of as the light purple area in Figure 1.3a, beyond the lines $q, p = a$. Figure 1.3b clarifies this to show a more global picture: we can imagine extending the ends of the asymptotes and hyperbola to join with each other, forming closed (non-intersecting) loops. Thus we visualise the symplectic invariant as being the light purple area shaded that exists between these two loops. This geometric construction is also detailed in [10].

The symplectic invariant σ represented by the lighter purple area is regular and does not exhibit logarithmic behaviour, unlike the area bounded between the phase trajectory (hyperbola) and the separatrices (axes). This is briefly discussed in [26] and it is mentioned that σ is an infinite Taylor series with no constant term.

1.3.2 Symplectic geometry

In the context of *symplectic geometry*, we define a *symplectic differential 2-form* ϖ. It is one which remains invariant under symplectic co-ordinate transformations (whose Jacobian is a linear *symplectic transformation* in the tangent space of the phase-space manifold $\mathcal{M}$ at some point $\mathbf{x} \in \mathcal{M}$, which we will denote by $T_{\mathbf{x}}\mathcal{M}$). The pair $(\mathcal{M}, \varpi)$ is called a *symplectic manifold*. So with such a bilinear form defined, it endows a geometry which we call *sym-*

plectic geometry, in a similar way that a scalar product endows a Euclidean space. This form induces a scalar skew-symmetric inner product, sometimes called a *skew-scalar* product $[\cdot,\cdot]$, whereby

$$[\mathbf{v}_1,\mathbf{v}_2] = -[\mathbf{v}_2,\mathbf{v}_1], \text{ and } [\mathbf{v},\mathbf{v}] = 0$$

for any vector inputs $\mathbf{v} \in T_{\mathbf{x}}\mathcal{M}$. Thus we define a linear symplectic transformation to be one which preserves the skew-scalar product. If $\mathbf{T} : \mathcal{M} \to \mathcal{M}$ is such a linear transformation then we have

$$[\mathbf{T}\mathbf{v}_1, \mathbf{T}\mathbf{v}_2] = [\mathbf{v}_1,\mathbf{v}_2].$$

One can show that we have two consequences, namely

$$\begin{aligned} \det \mathbf{T} &= 1 \\ \mathbf{T}^\top S \mathbf{T} &= S \end{aligned}$$

where S is the symplectic structure matrix.

Another concept useful in the following definition is *Morse theory*, whereby one is able to analyse the topology of a manifold using differentiable functions that have no degenerate critical points. Such functions are called *Morse functions*. A *Morse foliation* is one with isolated *Morse-type* singularities, whereby each singular leaf has exactly one singularity. Singularities of a Morse foliation whose leaves are levels of a Morse function are said to be of *Morse-type*.

1.3.3 Notions of equivalence

In this work the main aim is to calculate the semi-global symplectic invariants of the Euler top near the hyperbolic equilibrium point. In [8, 28] Dufour, Molino and Toulet introduce the classification of integrable systems using semi-global symplectic invariants. Their approach considers the triple $(\mathcal{M}, \varpi, \mathcal{F})$, where $\mathcal{M}$ is a two-dimensional manifold, ϖ is a symplectic differ-

ential 2-form, and $\mathcal{F}$ is a Morse foliation given by the levels of a Morse function F. Then the equivalence between two integrable Hamiltonian systems with one degree of freedom is introduced in [8] by the following definition.

Definition 1.1. Two triples $(\mathcal{M}_1, \varpi_1, \mathcal{F}_1)$ and $(\mathcal{M}_2, \varpi_2, \mathcal{F}_2)$ are said to be equivalent if there exists a symplectomorphism between $\mathcal{M}_1$ and $\mathcal{M}_2$ that preserves the foliation.

This means there exists a symplectic diffeomorphism $\Psi : \mathcal{M}_1 \to \mathcal{M}_2$ and a diffeomorphism $\Xi : \mathbb{R} \to \mathbb{R}$ such that

$$F_1 \circ \Psi = \Xi \circ F_2. \tag{1.11}$$

The semi-global symplectic invariant is introduced as the regular part of the action integral near a separatrix written in a particular canonical coordinate system defined using the Birkhoff normal form at the hyperbolic equilibrium point. The main theorem in [8] then is

Theorem 1.3. *In a full neighbourhood of a separatrix of the same topological type two systems are equivalent if and only if their semi-global symplectic invariants coincide.*

Remark 1.2. It should be noted that for C^∞ systems the relation (1.11) is not true, due to the presence of hyperbolic singularities. Furthermore, the symplectic invariant is the Taylor series of the regular part of the action integral only, and is not necessarily convergent. However we need not worry about these two issues, since both the Hamiltonian and Poisson structure of the Euler top are analytic.

1.3.4 A brief chronological review of the literature

[8] In 1994, Dufour, Molino and Toulet introduce a system for verifying equivalence of integrable systems on two dimensional manifolds (such as the Euler top). The triple $(\mathcal{M}, \varpi, \mathcal{F})$ is defined as per Section 1.3.3. The behaviour of the area bounded between the phase curves and the separatrices is studied for saddle equilibria.

The coefficients of the Taylor series about 0 of the regular parts of these areas are found to be invariants of the system when expressed in a special coordinate system that normalises the saddle.

[28] In 1996, Dufour's PhD student publishes her thesis expanding on the previous work. Toulet "obtains a complete classification system of integrable systems on two-dimensional symplectic manifolds" via the symplectic invariants introduced earlier. Hence, any integrable system on a two dimensional manifold can be uniquely classified up to equivalence of its symplectic invariants. Toulet provides hand-drawn diagrams similar to Figure 1.3a which illustrate the geometric interpretation of the symplectic invariant.

[23] In 2003, Vu Ngoc gives an extension of this classification for integrable systems of two degrees of freedom on four dimensional manifolds near *focus-focus* type equilibria.

[10] In 2007, Dullin and Vu Ngoc give a classification for integrable systems of two degrees of freedom on four dimensional manifolds near *hyperbolic-hyperbolic* type equilibria. The Neumann system is considered as a particular case to illustrate the general theory. The Birkhoff normal form is also computed via action integrals.

[9] In 2011, Dullin is the first to explicitly calculate the symplectic invariants for the spherical pendulum near the focus-focus singularity; it is an integrable system with two degrees of freedom on a four dimensional symplectic manifold. The Birkhoff normal form is calculated via both the Lie-series and action integrals. As a special case the pendulum is also studied.

[26] In 2012, Pelayo and Vu Ngoc find the linear approximation of the symplectic invariant near the focus-focus singularity of the spin-oscillator; their technique can be generalised to find terms of higher order. Other types of invariants (which are easier to find) are also studied. Later in the paper the quantization of the spin-oscillator is studied.

Chapter 2

Calculating the Birkhoff normal form

2.1 Introduction to normal forms

The theory of normal forms arises from a rather natural pursuit, which is to find a symplectic transformation which can remove as many terms as possible from a Hamiltonian. It turns out that this is possible, and the reduced Hamiltonian that has had such a symplectic transformation applied to it is said to be in *normal form*. Normal forms of Hamiltonians are covered in graduate texts, for example [1]. Here Arnold lists out the possible normal forms dependent upon the eigenvalues of the Hamiltonian system, and then goes on to define the Birkhoff normal form. Birkhoff himself in [2] develops normal forms in the neighbourhood of elliptic equilibria. Later others (for example Moser in [22]) consider normal forms at a hyperbolic equilibrium; it is the extension to the hyperbolic case that we are interested in studying in this work. An algorithm is presented in [20], which also presents a theorem with the conditions upon which the normal form is unique (which in our case it is).

2.2 Canonical variables

As it stands, our Hamiltonian $\tilde{\mathsf{H}}$ is a function of three non-canonical variables. Through a *Poisson map* $\mathbf{\Phi}$ we are able to write it as a function of two canonical variables - a (single) position and its conjugate momentum. A Poisson map is one which preserves the Poisson brackets. $\mathbf{\Phi}$ is a *symplectic map* if and only if its Jacobian $D\mathbf{\Phi}$ is symplectic. In essence it is the conservation of angular momentum and energy that allows us to reduce the Euler top to *one degree of freedom.* In order to calculate the Birkhoff normal form of the Hamiltonian of the Euler top at the unstable equilibrium, we introduce local canonical variables $(q, \tilde{p})$ with symplectic structure

$$S := \begin{pmatrix} 0 & 1 \\ -1 & 0 \end{pmatrix}.$$

Lemma 2.1. *The Poisson map* $\mathbf{\Phi} : \mathbb{R}^3 \to \mathbb{R}^2$ *defined by*

$$\mathbf{\Phi} = \begin{pmatrix} \Phi_1 \\ \Phi_2 \end{pmatrix} = \begin{pmatrix} q \\ \tilde{p} \end{pmatrix} = \begin{pmatrix} \operatorname{Arg}(L_2 + \mathrm{i}L_1) \\ L_3 \end{pmatrix}$$

maps the Hamiltonian $\tilde{\mathsf{H}}(\boldsymbol{L})$ *of* (1.3) *with value* $\tilde{\mathsf{h}}$ *and Poisson structure* $\hat{L}$ *on the symplectic leaf* $\mathcal{C}_\ell$ *into the standard symplectic structure* S *in canonical variables* $(q, \tilde{p})$ *and Hamiltonian* $\tilde{H}(q, \tilde{p})$ *with value* $\tilde{h}$ *given by*

$$\tilde{H}(q, \tilde{p}) = \frac{1}{2}\left[\tilde{p}^2\left(\Theta_3^{-1} - f(q)\right) - \ell^2\left(\Theta_2^{-1} - f(q)\right)\right] \tag{2.2}$$

where $f(q) := \Theta_1^{-1}\sin^2 q + \Theta_2^{-1}\cos^2 q$.

Proof. Substituting equations (2.1) into (2.2) and using $\ell^2 = L_1^2 + L_2^2 + L_3^2$ yields the required Hamiltonian (1.3) up to the constant $\frac{1}{2}\ell^2\Theta_2^{-1}$, such that $\tilde{H} \circ \mathbf{\Phi} + \frac{1}{2}\ell^2\Theta_2^{-1} = \tilde{\mathsf{H}}$. The hyperbolic equilibrium $\ell\hat{\boldsymbol{L}}_2$ is mapped to the origin $(q, \tilde{p}) = (0, 0)$, while $-\ell\hat{\boldsymbol{L}}_2$ is mapped to $(q, \tilde{p}) = (\pi, 0)$. To derive the new

symplectic structure, compute the 2×3 Jacobian matrix

$$\begin{aligned} D\boldsymbol{\Phi} &= \left(\frac{\partial \Phi_i}{\partial L_j}\right) \; i = 1, 2; \; j = 1, 2, 3 \\ &= \begin{pmatrix} \frac{L_2}{L_1^2+L_2^2} & -\frac{L_1}{L_1^2+L_2^2} & 0 \\ 0 & 0 & 1 \end{pmatrix} \end{aligned}$$

and verify that

$$\begin{aligned} D\boldsymbol{\Phi}\hat{L}\left(D\boldsymbol{\Phi}\right)^{\top} &= \begin{pmatrix} \frac{L_2}{L_1^2+L_2^2} & -\frac{L_1}{L_1^2+L_2^2} & 0 \\ 0 & 0 & 1 \end{pmatrix} \begin{pmatrix} 0 & -L_3 & L_2 \\ L_3 & 0 & -L_1 \\ -L_2 & L_1 & 0 \end{pmatrix} \begin{pmatrix} \frac{L_2}{L_1^2+L_2^2} & 0 \\ -\frac{L_1}{L_1^2+L_2^2} & 0 \\ 0 & 1 \end{pmatrix} \\ &= \begin{pmatrix} 0 & 1 \\ -1 & 0 \end{pmatrix} = S. \end{aligned}$$

□

Remark 2.1. The Hamiltonian in one degree of freedom can be readily found in the literature, for example in [14]. In our notation, Fassò writes the Hamiltonian as

$$\tilde{H}_{\text{Fassò}}(q, \tilde{p}) = \left(\frac{\cos^2 q}{2\Theta_1} + \frac{\sin^2 q}{2\Theta_2}\right)\left(\ell^2 - \tilde{p}^2\right) + \frac{\tilde{p}^2}{2\Theta_3}$$

and we find that

$$\tilde{H}_{\text{Fassò}}\left(q - \frac{\pi}{2}, \tilde{p}\right) - \frac{1}{2}\ell^2{\Theta_2}^{-1} = \tilde{H}(q, \tilde{p})$$

which is consistent with (2.2).

Note that this transformation to *cylindrical co-ordinates for the sphere* is not defined globally on sphere, but only on the punctured sphere with the two points $\pm\ell\hat{\boldsymbol{L}}_3$ (where $L_1 = L_2 = 0$) removed. However, the transformation is valid near the unstable equilibria $\pm\ell\hat{\boldsymbol{L}}_2$ and in a full neighbourhood of the separatrices.

Remark 2.2. At this stage it will be convenient to define the dimensionless

real parameters

$$\rho := \sqrt{\frac{\Theta_1}{\Theta_3}\frac{\Theta_3 - \Theta_2}{\Theta_2 - \Theta_1}} \tag{2.3a}$$

$$\kappa := \rho - \rho^{-1}, \tag{2.3b}$$

which will be fundamental in the upcoming analyses. Note that if $\rho \to \rho^{-1} \Leftrightarrow \kappa \to -\kappa$ are exchanged then $\Theta_1 \to \Theta_3$ are exchanged. The involution $\rho \to -\rho^{-1}$ leaves κ invariant. Furthermore, $\kappa^2 = \rho^2 - 2 + \rho^{-2}$ is rational in the moments of inertia. When restricting to the physical range $\rho > 0$, making ρ the subject in (2.3b) yields the unique injection $\rho = \frac{1}{2}(\kappa + \sqrt{\kappa^2 + 4})$. Since κ is such a fundamental parameter in the remainder of this work, we analyse it is growth and behaviour in more detail in Appendix B.

By taking advantage of Remark 2.2, we are now able to re-write our Hamiltonian (originally posed with three parameters) in terms of a single dimensionless parameter, and perform a non-dimensionalisation:

Lemma 2.2. *Using $\frac{1}{\lambda}$ as units of time, ℓ as units of angular momentum, and $\frac{\ell}{\lambda}$ as units of moment of inertia, the Hamiltonian in non-dimensional form is*

$$H(q,p) = \frac{1}{2}\left(-p^2\left(\rho + \rho^{-1}\sin^2 q\right) + \rho^{-1}\sin^2 q\right). \tag{2.4}$$

The proof is a simple calculation. The new scaled angular momentum $p = \frac{\tilde{p}}{\ell}$ is dimensionless, as is the value of the Hamiltonian $h = \frac{\tilde{h}}{\lambda\ell}$.

Remark 2.3. An alternative transformation introduces L_1 as momentum instead of L_3, and the corresponding Hamiltonian $\tilde{H}(q,\tilde{p})$ has Θ_1 and Θ_3 interchanged. That is, our map $\mathbf{\Phi}$ would be

$$\begin{aligned} q &= \operatorname{Arg}(L_2 - \mathrm{i}L_3) \\ \tilde{p} &= L_1 \end{aligned}$$

yielding the Hamiltonian

$$H(q,p) = \frac{1}{2}\left(p^2\left(\rho\sin^2 q + \rho^{-1}\right) - \rho\sin^2 q\right),$$

which can also be seen by applying the involution $\rho \to -\rho^{-1}$ to (2.4).

Remark 2.4. Each time a transformation occurs, the variables change. From here on in for clarity and simplicity of notation we use the same letters (q, p) for old and new variables, but it should be noted that each transformation introduces different variables. Recall that in our notation the tilde designates quantities with dimensions, while from this point onwards we use non-dimensionalised quantities H, q, h without tilde. Sans-serif font is used to designate quantities in the original Poisson system, so that $\tilde{\mathsf{h}} - \frac{1}{2}\ell^2 B = \tilde{h} = h\lambda\ell$.

Remark 2.5. When using cylindrical co-ordinates for the Casimir sphere $\mathcal{C}_\ell$, the area form on the original canonical cylinder $(q, \tilde{p}) \in [-\pi, \pi) \times (-\ell, \ell)$ in these variables is $\ell\, \mathrm{d}q \wedge \mathrm{d}\tilde{p} = \ell^2\, \mathrm{d}q \wedge \mathrm{d}p$. Hence the scaled *canonical symplectic form* on $\mathbb{R}^2$ is $\mathrm{d}q \wedge \mathrm{d}p$ and differs from the area form on the original Casimir sphere $\mathcal{C}_\ell$ by a factor of ℓ^2.

2.3 Discrete symmetry reduction

The original Hamiltonian has a group of discrete symmetries generated by $L_i \to -L_i$, $i = 1, 2, 3$. In the canonical variables these correspond to $q \to -q$, $q \to \pi - q$, $p \to -p$ respectively. The global analysis we are going to present later is simplest if there is only a single hyperbolic equilibrium on the separatrix in question, and therefore we are going to consider the Euler top modulo its discrete symmetry group. Any two pairs of the three discrete symmetries generate the group of symplectic discrete symmetries of the Euler top, which is isomorphic to Klein's Vierergruppe $V = \mathbb{Z}_2 \otimes \mathbb{Z}_2$. In the canonical variables a possible choice of generators is $\mathbf{S}_1(q, p) = (-q, -p)$ and $\mathbf{S}_2(q, p) = (\pi + q, p)$ which are both involutions. A fundamental region for the quotient of the cylindrical (q, p) phase space $[-\pi, \pi) \times (-1, 1)$ by the group V generated by $\mathbf{S}_1$ and $\mathbf{S}_2$ can be chosen as the positive quadrant

$(q,p) \in [0,\pi) \times [0,1)$. This corresponds to a quarter of the original sphere

$$V(\mathcal{C}_\ell) := \{\boldsymbol{L} \in \mathcal{C}_\ell \colon 0 < L_1 < \ell, -\ell < L_2 < \ell, 0 < L_3 < \ell\}.$$

2.4 Williamson normal form

We Taylor expand the non-dimensional Hamiltonian $H(q,p)$ about the origin $(q,p) = (0,0)$ for analysis near the equilibrium $\boldsymbol{L} = \ell\hat{\boldsymbol{L}}_2$. We do this by applying a *symlectic-with-multiplier* transformation $(q,p) \to \varepsilon(q,p)$ so that the equilibrium corresponds to $\varepsilon = 0$ and that is also the centre of our Taylor expansion. The result is

$$H(q,p) = \frac{\varepsilon^2}{2}\left(\rho^{-1}q^2 - \rho p^2\right) + \frac{\varepsilon^4\left(-3p^2q^2 - q^4\right)}{6\rho} + \mathcal{O}\left(\varepsilon^6\right).$$

The quadratic terms are $\frac{1}{2}(-p^2\rho + q^2\rho^{-1})$. The Williamson (linear) normal form of the hyperbolic equilibria is found after a symplectic linear transformation (for example as outlined in [5]). Although the Williamson normal form is unique up to the overall sign of the qp term (which we chose to be positive), the transformation is not. We chose to perform a symplectic scaling $q \to q\sqrt{\rho}, p \to p\sqrt{\rho^{-1}}$ followed by a rotation by $-\frac{\pi}{4}$, so that the positive quadrant in the new co-ordinates corresponds to positive Hamiltonian. With this convention the Williamson normal form becomes unique.

Lemma 2.3. *The symplectic linear transformation*

$$\begin{aligned}\begin{pmatrix} q \\ p \end{pmatrix} \;&\mapsto\; \begin{pmatrix} \sqrt{\rho} & 0 \\ 0 & \sqrt{\rho^{-1}} \end{pmatrix} \frac{1}{\sqrt{2}} \begin{pmatrix} 1 & 1 \\ -1 & 1 \end{pmatrix} \begin{pmatrix} q \\ p \end{pmatrix} \\ &= \frac{1}{\sqrt{2}} \begin{pmatrix} (p+q)\sqrt{\rho} \\ (p-q)\sqrt{\rho^{-1}} \end{pmatrix}\end{aligned}$$

gives the Williamson's normal form H_* of the Hamiltonian H as

$$H_* = \varepsilon^2 qp + \varepsilon^4\left(-\frac{\left(p^2-q^2\right)^2}{8\rho} - \frac{1}{24}\rho(p+q)^4\right) + \mathcal{O}\left(\varepsilon^6\right).$$

We define the leading order term $qp =: J$, where q, p are the canonical variables *after* the linear transformation has been performed. Notice that

$$\begin{aligned} J &= qp \text{ (in terms of the new canonical scaled variables)} \\ &= \frac{1}{2}\left(p^2 - q^2\right) \text{ (old canonical scaled variabes)} \\ &= \frac{1}{2}\left(\frac{\tilde{p}^2}{\ell^2} - q^2\right) \text{ (old canonical unscaled variables)} \\ &= \frac{1}{2}\left(\frac{L_3^2}{\ell^2} - \left[\operatorname{Arg}\left(L_2 + \mathrm{i}L_1\right)\right]^2\right) \text{ (original non-canonical variables).} \end{aligned}$$

2.5 The Lie transform algorithm

Having obtained Williamson's normal form of the Hamiltonian, in order to arrive at the Birkhoff normal form, we use the method of Lie transforms to remove terms that are not powers of $J = qp$. We proceed in a manner outlined in [20].

Consider a near-identity symplectic change of variables $\boldsymbol{y} \mapsto \boldsymbol{X}$ that depends upon a small parameter ε such that $\boldsymbol{X}(\varepsilon, \boldsymbol{y}) = \boldsymbol{y} + \mathcal{O}(\varepsilon)$ with near-identity symplectic inverse $\boldsymbol{Y}(\varepsilon, \boldsymbol{x}) = \boldsymbol{x}(\varepsilon) + \mathcal{O}(\varepsilon)$. Then there exists a smooth function W that satisfies the Hamiltonian system

$$\frac{\mathrm{d}\boldsymbol{x}}{\mathrm{d}\varepsilon} = S\boldsymbol{\nabla}W,\ \boldsymbol{x}(0) = \boldsymbol{y}. \tag{2.5}$$

More to the point, we wish to generate a near-identity symplectic change of variables $\boldsymbol{X}$ which is the solution to (2.5) and removes as many terms as possible. The general theory states that we cannot remove terms that are powers of J, but we can remove all other terms. From the above, [20] comments that Hamiltonian systems generate symplectic coordinate transformations *directly*. Thus the generating function which produces such a change of variables is a polynomial with coefficients chosen in such a way as to eliminate all the terms that are not powers of J.

Below are the some preliminary definitions and notations:

H_*	Williamson's normal form of the Hamiltonian, before the Lie transform has been applied
H_i^0	The term of degree i in q and p in H_*
H^*	The Lie-transform of the Hamiltonian H_* generated by W, as a function of J only (Birkhoff normal form)
H_0^i	The term of degree i in q and p (and hence $\frac{i}{2}$ in J) in H_*
W	A smooth function that generates the Lie transformation
W_i	The generating function of order i. It is a polynomial in q and p with terms of degree $2(i+1)$ eliminating terms of order $2(i+1)$ in q and p in H_i^0.

Using the above definitions we have

$$\begin{aligned} H_* &= \sum_{i=0}^{\infty} \frac{\varepsilon^i}{i!} H_i^0 \\ H^* &= \sum_{i=0}^{\infty} \frac{\varepsilon^i}{i!} H_0^i \\ W_i &= \sum_{k=0}^{2(i+1)} \nu_{i,k} q^k p^{2(i+1)-k} \\ W &= \sum_{i=0}^{\infty} \frac{\varepsilon^i}{i!} W_{i+1} \end{aligned}$$

for some constants $\nu_{i,k}$ to be determined by solving the elimination conditions. To facilitate in the computation of the algorithm, the doubly-indexed array $\left\{H_j^i\right\}_{i,j\in\mathbb{N}}$ is introduced.

Remark 2.6. Earlier we performed a scaling by ε. This does not cause any concern, as we were only after a formal series in the interim. We may later apply the inverse transformation $(q,p) \to \varepsilon^{-1}(q,p)$ or simply set $\varepsilon = 1$.

The below Lemma contains the recursive algorithm as given in [20].

Lemma 2.4. *The Lie transform generated by W transforms Williamson's normal form H_* into the Birkhoff normal form H^* using the double-indexed array $\left\{H_j^i\right\}_{i,j\in\mathbb{N}}$ related recursively via*

$$H_j^i = H_{j+1}^{i-1} + \sum_{k=0}^{j} \binom{j}{k} \left\{H_{j-k}^{i-1}, W_{k+1}\right\}$$

where $\{\cdot,\cdot\}$ is the Poisson bracket in canonical co-ordinates (q,p).

The algorithm is implemented in Mathematica; we state the main results in the following Theorem.

Theorem 2.1. *The Birkhoff normal form up to order 4 of the Euler top at the hyperbolic equilibrium point is given by*

$$H^*(J) \;=\; J - \frac{\kappa}{4}J^2 - \frac{\kappa^2+4}{16}J^3 - \frac{5\kappa\left(\kappa^2+4\right)}{128}J^4 + \mathcal{O}\left(J^5\right) \qquad (2.6)$$

where $J := qp$ in the new variables.

More terms up to order 10 are given in Appendix A.1. Note that the parameter dependence is only through the dimensionless parameter κ and the power series is in terms of the dimensionless action J.

The Birkhoff normal form about a hyperbolic equilibrium point has two nice properties. Firstly, Birkhoff in [2] asserts that (in our notation) if $H_0^0 \propto J$ then given a particular H_* the resultant Birkhoff normal form is unique. Even more interesting is the theorem of Moser in [22], namely when the origin is a *general hyperbolic point*, then the symplectomorphism $H_* \mapsto H^*$ converges implies that the Birkhoff normal form converges. Just recently in 2005 Zung proved in [30] that for an analytic integrable system, the Birkhoff normal form is convergent. For us our (symmetry-reduced) Euler top has one degree of freedom and so is automatically integrable (as is the full system in any case). Combined with the fact that the Euler top is analytic, we can then conclude that the Birkhoff normal form must converge. We will see numerical confirmation of this in Section 5.

Chapter 3

Action integrals via Picard-Fuchs equation

The action integrals are represented by the areas enclosed by closed orbits in phase space, as illustrated by the comparison in Figure 3.1. We initially calculate the actions as areas on both the quarter Casimir sphere $\boldsymbol{L} \in V(\mathcal{C}_\ell)$ in Figure 3.1a, and on the scaled and discrete symmetry reduced canonical phase plane $(q, p) \in [0, \pi) \times [0, 1)$ in 3.1b. The thick black line is the separatrix with $h = 0$. The light blue and dark red shaded areas below and above the separatrix respectively show the actions of orbits with $h > 0$ and $h < 0$ respectively. The symplectic invariant is calculated from these areas in the singular limit $h \to 0$.

The essential step in the calculation of the semi-global symplectic invariants is the computation of the action integrals, which are given by complete elliptic integrals in the case of the Euler top. Since we are interested in the series expansions of these integrals the most natural approach is not through the integral itself, but instead through the so called *Picard-Fuchs* ODE that the integral satisfies. The derivation of the Picard-Fuchs equation proceeds in a way similar to [11]. Frobenius expansions of this linear ODE then gives the desired series. This gives a basis for the vector space of solutions of the

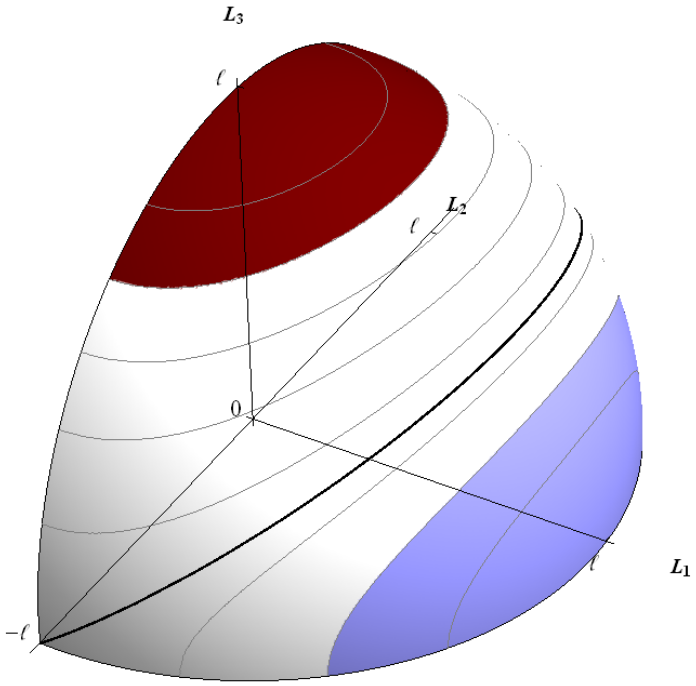

(a) Discrete symmetry reduced Casimir sphere $V(\mathcal{C}_\ell)$

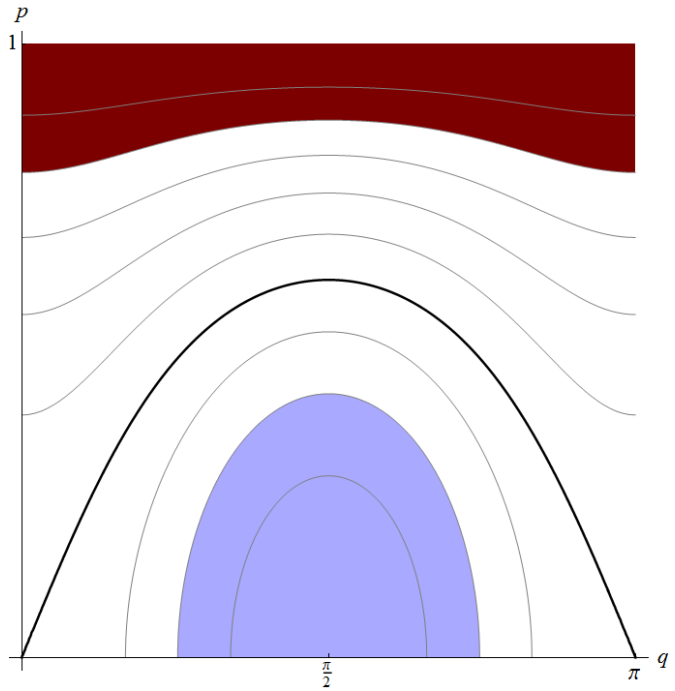

(b) Discrete symmetry reduced canonical phase plane

Figure 3.1: Comparison of areas enclosed by the same closed orbits after discrete symmetry reduction with parameter value $\kappa = 0.5$.

linear ODE, and in a second step the particular solutions corresponding to the action integrals of the Euler top are found.

3.1 Calculation of the action integrals

Lemma 3.1. *The scaled and discrete symmetry reduced action of the Euler top with scaled energy h normalised to 0 at the unstable equilibrium is a complete elliptic integral on the curve*

$$\Gamma := \{(z,u) \in \mathbb{C}^2 \,|\, u^2 = (2h-z)w^2, \quad [w(z)]^2 = z(z^2+\kappa z - 1)\}$$

given by

$$I_{\beta_\pm}(h) = \frac{1}{4\pi} \oint_{\beta_\pm} \frac{\sqrt{2h-z}}{w(z)} \, \mathrm{d}z$$

along the cycles $\beta_\pm$ for $\pm h > 0$ as specified in Figure 3.2.

Before we proceed with the proof, we establish some conventions. We choose two linearly-independent curves which disconnect the elliptic curve Γ (which is a torus). We denote these α and β, which give rise to the imaginary and real actions respectively. The (finite) branch points are $z \in \{2h, 0, -\rho, \rho^{-1}\}$. For the case $-\rho < 0 < 2h < \rho^{-1}$ denote the cycles by α_+, β_+, whilst for the case $-\rho < h < 0 < \rho^{-1}$ denote the cycles by α_-, β_-. There are two branch cuts to be fixed. We take them to be in the intervals $(-\rho, \rho^{-1}) \setminus [\min\{0, 2h\}, \max\{0, 2h\}]$. The cycles are chosen such that β encloses the branch cut along the real interval between $2h$ and the other nearest non-zero branch point, whilst α encloses the real interval between 0 and $2h$. The β-cycles can be shrunk down, so that we are integrating along the real intervals $\Pi[\beta_+] := (2h, \rho^{-1})$ and $\Pi[\beta_-] := (-\rho, 2h)$. We are allowed to do this because the integrand is holomorphic everywhere except the branch cuts and branch points.

Proof. We derive the action using the Hamiltonian $H(q,p)$ in canonical variables (q,p). Solving $H(q,p) = h$ for p and integrating with respect to q in

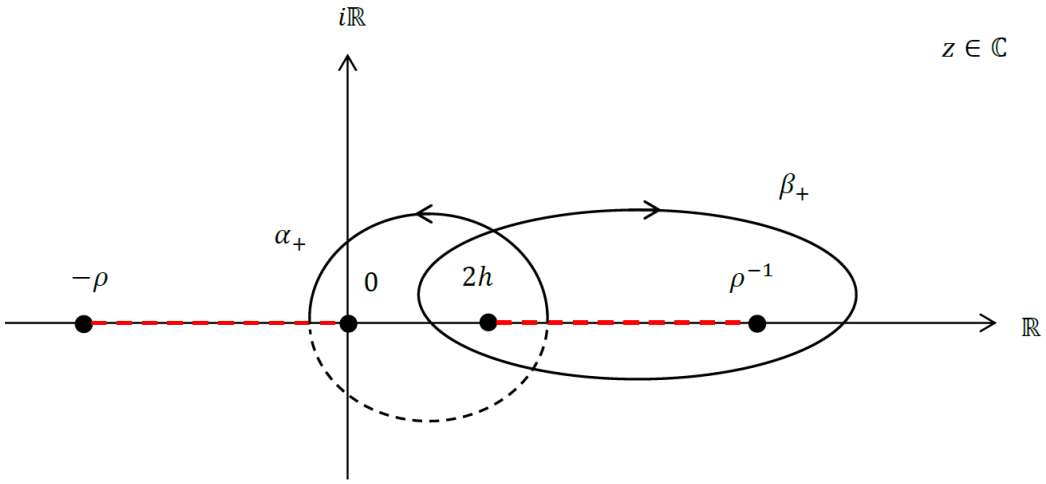

(a) $h > 0$

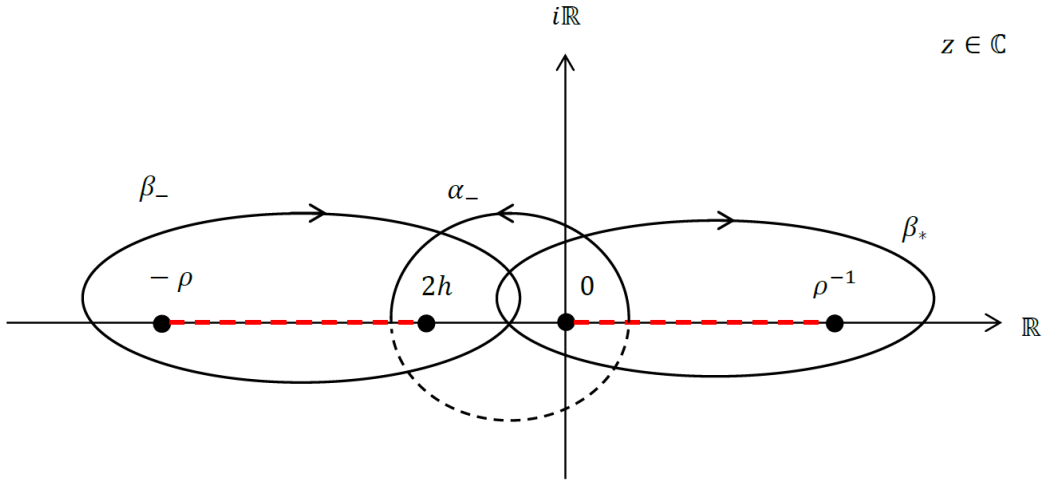

(b) $h < 0$

Figure 3.2: The α and β-cycles, choices of branch cuts and branch points of Γ in the $z \in \mathbb{C}$ plane for $\pm h > 0$. The reader should note that upon calculation of the contour integrals, these cycles are shrunk until they sit entirely upon the real axis; they are shown here in their "pre-shrunken" form.

order to find the lighter blue area in Figure 3.1 gives

$$I_{\beta_+}(h) = \frac{1}{2\pi} \int_{q_0}^{\pi - q_0} \sqrt{-\frac{2h - \rho^{-1}\sin^2 q}{\rho + \rho^{-1}\sin^2 q}}\, \mathrm{d}q$$

where $q_0 = \sin^{-1}(\sqrt{2h\rho})$. Upon performing the change of integration variable $z = \rho^{-1}\sin^2(q)$ we arrive at the required integral over the differential 1-form

$$\zeta(h) := \frac{\sqrt{2h - z}}{w(z)}\, \mathrm{d}z.$$

The new denominator is defined to be

$$[w(z)]^2 := z\left(z^2 + \kappa z - 1\right) = z(z + \rho)(z - \rho^{-1})$$

and depends only upon the single parameter $\kappa = \rho - \rho^{-1}$. Note that on Γ we find $\zeta = \frac{u}{w^2}\, \mathrm{d}z$ is meromorphic, so then we can equate the real integral over $z \in [q_0, \pi - q_0] \subset \mathbb{R}$ to an equivalent complex contour integral over $z \in \beta_+ \subset \mathbb{C}$, namely

$$\int_{q_0}^{\pi - q_0} \zeta = \frac{1}{2} \oint_{\beta_+} \zeta,$$

which is evaluated by continuously shrinking β_+ so that it sits entirely upon the real axis. We find that β_+ gives two equal contributions as z traverses each side of the branch cut. Then, q traversing the interval $[q_1, q_2]$ once corresponds to z traversing the whole closed (shrunken) path β_+ once. Thus the complex closed loop integral around β_+ gives twice the real integral along the interval $\Pi[\beta_+]$, and so altogether $I_{\beta_+} = \frac{1}{4\pi} \oint_{\beta_+} \zeta$.

A slightly more complicated argument applies in the case $h < 0$. To get the lighter shaded (red) area in Figure 3.1 the integrand is $(1 - p)\, \mathrm{d}q$ instead of just $p\, \mathrm{d}q$ and the real integration interval is $q \in [0, \pi]$. Let $\gamma_\infty, \beta_-, \beta_*$ be clockwise contours enclosing $\infty \in \mathbb{C}^\star, \Pi[\beta_-], [0, \frac{1}{\rho}]$ respectively. Then $\gamma_\infty \cup \beta_- \cup \beta_*$ is a clockwise contour enclosing all singular points on the

Riemann sphere, and we have

$$\begin{aligned}\oint_{\gamma_\infty} + \oint_{\beta_-} + \oint_{\beta_*} &= 0\\ \Rightarrow \oint_{\beta_*} &= -\oint_{\gamma_\infty} - \oint_{\beta_-}\end{aligned}$$

and so, from the above definition of the action

$$\begin{aligned}I_{\beta_-}(h) &= \frac{1}{2\pi}\int_0^\pi (1-p)\,\mathrm{d}q\\ &= \frac{1}{2} - \frac{1}{2\pi}\int_0^\pi \frac{\sqrt{\rho^{-1}\sin^2 q - 2h}}{\sqrt{\rho + \rho^{-1}\sin^2 q}}\,\mathrm{d}q\\ &= \frac{1}{2} - \frac{1}{2\pi}\int_0^{\rho^{-1}} \frac{\sqrt{2h-z}}{\sqrt{z(z+\rho)(z-\rho^{-1})}}\,\mathrm{d}z\\ &= \frac{1}{2} - \frac{1}{2}\frac{1}{2\pi}\oint_{\beta_*} \frac{\sqrt{2h-z}}{\sqrt{z(z+\rho)(z-\rho^{-1})}}\,\mathrm{d}z.\end{aligned}$$

Now we calculate the integral that encloses infinity. Using the residue at infinity we have

$$\frac{1}{2\pi}\oint_{\gamma_\infty} \zeta = -\frac{1}{2\pi} 2\pi \mathrm{i} \operatorname*{Res}_\infty \zeta = -\mathrm{i}\times -\mathrm{i} = -1,$$

and finally we have

$$\begin{aligned}I_{\beta_-}(h) &= \frac{1}{2} - \frac{1}{2}\left(1 - \frac{1}{2\pi}\oint_{\beta_-}\zeta\right)\\ &= \frac{1}{4\pi}\oint_{\beta_-} \frac{\sqrt{2h-z}}{\sqrt{z(z+\rho)(z-\rho^{-1})}}\,\mathrm{d}z\end{aligned}$$

so indeed we have the expected result. □

Remark 3.1. The unscaled action $\tilde{I}$ as a function of the unscaled and unshifted energy $\tilde{\mathsf{h}}$ can be rewritten in the symmetric form

$$\tilde{I}_{\beta_\pm}\left(\tilde{\mathsf{h}}, \ell\right) = \frac{1}{2\pi}\oint_{\beta_\pm} \sqrt{-\frac{2\tilde{\mathsf{h}} - \ell^2\tilde{z}}{\left(\tilde{z} - \Theta_1^{-1}\right)\left(\tilde{z} - \Theta_2^{-1}\right)\left(\tilde{z} - \Theta_3^{-1}\right)}}\,\mathrm{d}\tilde{z} = 2\ell I_{\beta_\pm}(h)\,.$$

The scaled action I depends on $\tilde{\mathsf{h}}$ and ℓ only through

$$h = \frac{\tilde{\mathsf{h}} - \frac{1}{2}\Theta_2^{-1}\ell^2}{\lambda\ell},$$

and on Θ_i only through κ. In the transformed variable the roots $\tilde{z} = \Theta_1^{-1}, \Theta_2^{-1}, \Theta_3^{-1}$ correspond to the roots $z = -\rho, 0, \rho^{-1}$ of w, respectively.

3.2 Derivation of the Picard-Fuchs equation

We now derive the Picard-Fuchs ODE of $I(h)$. ζ is an Abelian differential living on the complex manifold Γ. By de Rham cohomology theory, there must exist a relationship between derivatives of ζ on Γ. In fact, we follow the route of Clemens in [7] and find that there exists a linear combination of the derivatives of ζ that equals a total differential. However, we cannot exploit the same simplifications as Clemens does since our independent variable is fixed to be the energy h, because otherwise we would lose the connection to the Birkhoff normal form (see Section 4.1). A similar approach was taken in [11]. The relation between the differentials is given in the following Lemma.

Lemma 3.2. *There exists a function $F(z)$ meromorphic on Γ and coefficients c_i such that*

$$\sum_{i=0}^{3} c_i \frac{\mathrm{d}^i\zeta}{\mathrm{d}h^i} = \mathrm{d}F. \tag{3.1}$$

Proof. Observe that

$$\begin{aligned} w(z)(2h-z)^{\frac{5}{2}} \sum_{i=0}^{3} c_i \frac{\mathrm{d}^i\zeta}{\mathrm{d}h^i} &= \left[-c_0 z^3 + (6c_0 h + c_1)z^2 + (-12c_0h^2 - 4c_1 h + c_2)z \right. \\ &\quad \left. + (8c_0h^3 + 4c_1h^2 - 2c_2h + 3c_3)\right]. \end{aligned} \tag{3.2}$$

Now choose $F(z) := \dfrac{u}{(2h-z)^2} = \dfrac{w(z)}{(2h-z)^{\frac{3}{2}}}$, which is meromorphic on Γ (since it is rational in u and z) and has differential

$$w(z)(2h-z)^{\frac{5}{2}}\mathrm{d}F = \left[(3h + \tfrac{1}{2}\kappa)z^2 + (2\kappa h - 1)z - h\right]\mathrm{d}z. \tag{3.3}$$

Equating coefficients of the polynomials of z in (3.2) and (3.3) and solving for the c_i yields the unique solution

$$\begin{aligned} c_0 &= 0 \\ c_1 &= 3h + \frac{\kappa}{2} \\ c_2 &= 12h^2 + 4\kappa h - 1 \\ c_3 &= h(4h^2 + 2h\kappa - 1) = \frac{1}{2}\left[w(2h)\right]^2. \end{aligned}$$

Thus by construction we have proven the Lemma. □

Now we are ready to derive the linear and homogeneous Picard-Fuchs equation for the action $I(h)$.

Theorem 3.1. *The scaled action $I(h)$ satisfies the Picard-Fuchs equation*

$$\left[w(2h)\right]^2 I'''(h) + 2(12h^2 + 4\kappa h - 1)I''(h) + (6h + \kappa)I'(h) = 0 \qquad (3.4)$$

with the scaled energy $h \in \mathbb{R}$ as the independent variable.

Proof. To obtain the Picard-Fuchs ODE, perform a closed complex contour integral to both sides of equation (3.1). By definition we have $\oint \zeta = 4\pi I$, and given F is meromorphic on Γ the residues of $\mathrm{d}F$ are vanishing, so that the right hand side gives $\oint \mathrm{d}F = 0$ for any closed integration path. □

3.3 Solving the Picard-Fuchs equation

Clearly (3.4) is an ODE in I' thus $I = k_3$ is a constant solution. To lower the order we introduce the scaled period $T(h) = 2\pi I'(h)$, which has the first kind differential $\frac{\mathrm{d}z}{u}$ on Γ. The scaled period $T(h)$ hence satisfies the second order linear homogeneous ODE

$$T''(h) + 2\frac{12h^2 + 4\kappa h - 1}{\left[w(2h)\right]^2}T'(h) + \frac{6h + \kappa}{\left[w(2h)\right]^2}T(h) = 0. \qquad (3.5)$$

It is interesting to observe that the leading coefficient c_3 is proportional to $\left[w(2h)\right]^2$, and thus in normalising the ODE the roots of $w(2h)$ given by

$2h \in \{0, -\rho, \rho^{-1}\}$ become the (regular) singular points of the Picard-Fuchs ODE, also corresponding to the branch points of Γ. Thus the partial fraction decomposition of the coefficient of T' simply is

$$2\left(\frac{1}{2h} + \frac{1}{2h+\rho} + \frac{1}{2h-\rho^{-1}}\right).$$

We are interested in series solutions at the singular point corresponding to the unstable equilibrium, namely $h = 0$. The general theory and procedure for solving (3.5) via the method of Frobenius can for example be found in [6]. We seek series solutions of the form

$$\sum_{n=0}^{\infty} a_n(\varrho) h^{n+\varrho} \tag{3.6}$$

where ϱ is a root of the indicial equation. At the finite singular points the indicial equation is $\varrho^2 = 0 \Rightarrow \varrho = 0, 0$.

Remark 3.2. We should also consider the singular point at infinity. Perform a change of variables $\eta = \frac{1}{h}$, $\tau(\eta) = T(\frac{1}{h})$ to yield

$$\begin{aligned} \tau''(\eta) - 2\frac{\eta^2+4}{\eta^4 w\left[\frac{2}{\eta}\right]^2}\tau'(\eta) + \frac{\eta\kappa+6}{\eta^5 w\left[\frac{2}{\eta}\right]^2}\tau(\eta) &= 0 \\ \Leftrightarrow \tau''(\eta) - \frac{\rho\,(\eta^2+4)}{\eta(2\rho-\eta)(\eta\rho+2)}\tau'(\eta) + \frac{\eta\rho^2+6\rho-\eta}{2\eta^2(2\rho-\eta)(\eta\rho+2)}\tau(\eta) &= 0. \end{aligned}$$

This type of transformation is found in texts such as [29]. Clearly $\eta = 0$ is a regular singular point of the transformed ODE; the coefficient of τ' has a single pole and that of τ a double pole at $\eta = 0$. Hence the original Picard-Fuchs ODE has a regular singular point at $h = \infty$. The indicial equation for the singular point at infinity can be found by calculating the indicial equation for $\eta = 0$ of the transformed equation. It is given by

$$\varrho_\infty^2 - 2\varrho_\infty + \tfrac{3}{4} = 0$$

and yields indicial roots $\varrho_\infty = \frac{1}{2}, \frac{3}{2}$, differing by an integer. This shows us

that the transformed equation is also Fuchsian.

By substitution of the Frobenius series (3.6) into the ODE (3.5), the recursion relation for $a_n(\varrho)$ is found to be

$$a_n(\varrho) = \frac{2n+2\varrho-1}{(n+\varrho)^2}\left(\frac{\kappa}{2}(2n+2\varrho-1)a_{n-1}(\varrho) + (2n+2\varrho-3)a_{n-2}(\varrho)\right) \tag{3.7}$$

Setting $\varrho = 0$ and defining $a_n := a_n(0)$ in (3.6) yields the Frobenius expansion of the regular solution

$$T_r(h) = \sum_{n=0}^{\infty} a_n h^n$$

with coefficients obtained from (3.7) at $\varrho = 0$ as

$$a_n = \frac{2n-1}{n^2}\left(\frac{\kappa}{2}(2n-1)a_{n-1} + (2n-3)a_{n-2}\right). \tag{3.8}$$

Since we have a single value for ϱ, we can remove the dependence of the coefficients $a_n(\varrho)$ on ϱ, which is why we simply write a_n. We solve this second order recursion relation for a_n. Without loss of generality, we normalise the initial condition $a_0 := 1$, and require that $a_{-1} := 0$. Thus we find that the next few coefficients are

$$\begin{aligned}
a_1 &= \frac{\kappa}{2}, \\
a_2 &= \frac{3}{16}\left(3\kappa^2+4\right), \\
a_3 &= \frac{5}{32}\kappa\left(5\kappa^2+12\right), \\
a_4 &= \frac{35}{1024}\left(35\kappa^4+120\kappa^2+48\right), \\
a_5 &= \frac{63\kappa}{2048}\left(63\kappa^4+280\kappa^2+240\right).
\end{aligned}$$

Theorem 3.2. *The recursion for a_n is solved by*

$$a_n = \frac{1}{4^n}\binom{2n}{n}\sum_{k=0}^{\lfloor \frac{n}{2} \rfloor}\binom{2n-2k}{k, n-k, n-2k}\left(\frac{\kappa}{2}\right)^{n-2k} \tag{3.9}$$

where $\binom{n}{i,j,k} = \frac{n!}{i!j!k!}$ *with* $n = i + j + k$ *is the trinomial coefficient.*

The proof of this theorem will be given later as a special case of the (approximate) solution of the more general recursion for $a_n(\varrho)$.

Remark 3.3. It is interesting to note that the sum a_n can be summed to the hypergeometric function ${}_2F_1$

$$a_n = 8^{-n}\left(\frac{(2n)!}{(n!)^2}\right)^2 \kappa^n \, {}_2F_1\left(-\frac{n-1}{2}, -\frac{n}{2}; -\frac{2n-1}{2}; -\frac{4}{\kappa^2}\right)$$

which is always terminating because n is an integer. The solution T of (3.5) is a complete elliptic integral of first kind, can be expressed in terms of the hypergeometric function as the function of the modulus of the elliptic curve. Interestingly, the coefficients of the Taylor series of $T_r(h)$ are also given by the hypergeometric function.

Since we have repeated indicial roots, we expect the second independent solution to be singular. The general theory (see for example [6]) says that the singular solution is of the form

$$T_s(h) := T_r(h)\ln|h| + \sum_{n=1}^{\infty} b_n h^n$$

where $b_n := \left.\frac{\mathrm{d}a_n(\varrho)}{\mathrm{d}\varrho}\right|_{\varrho=0}$. The recursion relation for b_n at $\varrho = 0$ is thus given by

$$b_n = \frac{(2n-1)\left(2\kappa a_{n-1} + \kappa n(2n-1)b_{n-1} + 2n(2n-3)b_{n-2}\right) + 4(4n-3)a_{n-2}}{2n^3}. \tag{3.10}$$

Along with the initial conditions on the a_n, we also impose that $b_{-1} := 0$ and

(from the general theory) $b_0 := 0$. The first few coefficients are

$$\begin{aligned} b_1 &= \kappa, \\ b_2 &= \frac{1}{16}\left(21\kappa^2 + 20\right), \\ b_3 &= \frac{1}{96}\kappa\left(185\kappa^2 + 372\right), \\ b_4 &= \frac{1}{6144}\left(18655\kappa^4 + 56760\kappa^2 + 18672\right), \\ b_5 &= \frac{1}{20480}\kappa\left(102501\kappa^4 + 416360\kappa^2 + 313680\right). \end{aligned}$$

We were not able to find an explicit solution for $a_n(\varrho)$. However, since we only need the derivative for $a_n(\varrho)$ at $\varrho = 0$ it is enough to find an approximate solution $\hat{a}_n(\varrho)$ that is valid up to terms of $\mathcal{O}(\varrho^2)$.

Lemma 3.3. *The recursion for $a_n(\varrho)$ given by (3.7) is solved by*

$$\hat{a}_n(\varrho) = 2^n \kappa^n n! \frac{\left(\varrho + \frac{1}{2}\right)_n}{(\varrho+1)_n^2} \sum_{k=0}^{\lfloor \frac{n}{2} \rfloor} \frac{\left(\varrho + \frac{1}{2}\right)_{n-k}}{(n-2k)!k!} \kappa^{-2k}$$

to leading order in ϱ, where $(x)_n$ is the Pochhammer symbol.

Note that this formula reduces to the explicit formula for a_n given earlier when $\varrho = 0$ using the identity

$$\left(\frac{1}{2}\right)_n = \frac{(2n-1)!}{2^{2n-1}(n-1)!}.$$

Hence the following proof will also prove Theorem 3.2.

Proof. We will show that $a_n(\varrho) = \hat{a}_n(\varrho) + \mathcal{O}(\varrho^2)$ by induction. From the explicit recursion we find

$$a_1(\varrho) = \frac{(1+2\varrho)^2}{2(1+\varrho)^2}\kappa$$

and

$$a_2(\varrho) = \frac{(1+2\varrho)(3+2\varrho)}{(2+\varrho)^2} + \frac{(1+2\varrho)^2(3+2\varrho)^2}{4(1+\varrho)^2(2+\varrho)^2}\kappa^2.$$

One can easily check that $a_1(\varrho) = \hat{a}_1(\varrho)$, Furthermore, the coefficients of κ^2 in $a_2(\varrho)$ and $\hat{a}_2(\varrho)$ coincide and the constant and linear coefficients of $a_2(\varrho)$ and $\hat{a}_2(\varrho)$ are both

$$\tfrac{3}{4} + \tfrac{5}{4}\varrho + \mathcal{O}(\varrho^2).$$

Now assume that the identity $a_n(\varrho) = \hat{a}_n(\varrho) + \mathcal{O}(\varrho^2)$ holds for all $1 \leq n \leq m-1$ for some fixed $2 \leq m \in \mathbb{N}$. Thus we aim to show that under these assumptions, $a_m(\varrho) = \hat{a}_m(\varrho) + \mathcal{O}(\varrho^2)$ holds. In order to show that this is true we need to show that the Taylor series of the factor multiplying $\mathcal{O}(\varrho^2)$ has a non-zero constant term. We substitute the formulas $\hat{a}_{m-1}(\varrho)$ and $\hat{a}_{m-2}(\varrho)$ into the right hand side of (3.7) with $n = m$ and need to verify that $a_m(\varrho)$ so obtained is equal to $\hat{a}_m(\varrho) + \mathcal{O}(\varrho^2)$.

For simplicity, define $d_m := a_m(\varrho)(2m + 2\varrho + 1)$ so that

$$d_m = g_m(\tfrac{\kappa}{2}d_{m-1} + d_{m-2}), \quad \text{where } g_m := \frac{(2m+2\varrho+1)(2m+2\varrho-1)}{(m+\varrho)^2}\,.$$

Using the formula for $\hat{a}_m$ and the above definition of d_m we define a related $\hat{d}_m$ which can be written as

$$\hat{d}_m := \hat{a}_m(\varrho)(2m+2\varrho+1) = G_m(\varrho)\sum_{k=0}^{\lfloor \frac{m}{2} \rfloor} S_{m,m-2k}(\varrho)\kappa^{m-2k},$$

where

$$G_m(\varrho) := \frac{2^{m+1}m!\left(\varrho+\frac{1}{2}\right)_{m+1}}{(\varrho+1)_m^2}, \quad S_{i,j}(\varrho) := \frac{\left(\varrho+\frac{1}{2}\right)_{\frac{i+j}{2}}}{\left(\frac{i-j}{2}\right)!j!}\,.$$

The equivalent claim is that

$$\begin{aligned} d_m &= \hat{d}_m + \mathcal{O}(\varrho^2) \\ \Rightarrow \hat{d}_m &= g_m(\tfrac{\kappa}{2}\hat{d}_{m-1} + \hat{d}_{m-2}) + \mathcal{O}(\varrho^2). \end{aligned} \tag{3.11}$$

Inserting the series for $\hat{d}$ and collecting powers of κ gives

$$G_m(\varrho)S_{m,m-2k}(\varrho) = g_m\left(\tfrac{1}{2}G_{m-1}(\varrho)S_{m-1,m-2k-1}(\varrho) + G_{m-2}(\varrho)S_{m-2,m-2k}(\varrho)\right) + \mathcal{O}(\varrho^2)\,.$$

Dividing the above equation by $G_{m-1}(\varrho)S_{m-2,m-2k}(\varrho)$ and using the identities

$$\frac{G_m(\varrho)}{G_{m-1}(\varrho)} = \frac{m(2m+2\varrho+1)}{(m+\varrho)^2} = \frac{m}{2m+2\varrho-1}g_m$$

and

$$\frac{S_{m,m-2k}(\varrho)}{S_{m-2,m-2k}(\varrho)} = \frac{2m-2k+2\varrho-1}{2k}, \quad \frac{S_{m-1,m-2k-1}(\varrho)}{S_{m-2,m-2k}(\varrho)} = \frac{m-2k}{k},$$

we have (after some simplification)

$$\frac{m}{2m+2\varrho-1} = 1 - \frac{(m+\varrho-1)^2}{(m-1)(2m+2\varrho-1)} - \frac{\mathcal{O}\left(\varrho^2\right)}{G_{m-1}(\varrho)S_{m-2,m-2k}(\varrho)}.$$

Re-arranging for ϱ^2 gives us

$$\varrho^2 = -\frac{(m-1)(2m+2\varrho-1)}{G_{m-1}(\varrho)S_{m-2,m-2k}(\varrho)}\mathcal{O}\left(\varrho^2\right).$$

Evaluating the coefficient of $\mathcal{O}\left(\varrho^2\right)$ at $\varrho = 0$ gives

$$-\frac{(m-1)(2m-1)}{G_{m-1}(0)S_{m-2,m-2k}(0)} = -\frac{\left(2m^2-3m+1\right)(k-1)!(m-1)!(m-2k)!}{2^m\left(\frac{1}{2}\right)_m\left(\frac{1}{2}\right)_{m-k-1}},$$

which is non-zero for all integers $0 \leq k \leq \left\lfloor \frac{m}{2} \right\rfloor$, $m \geq 2$ and hence the the Taylor series of the factor multiplying $\mathcal{O}\left(\varrho^2\right)$ has a non-zero constant term. This shows that for each power of κ in (3.11) the estimation holds, and thus it holds for the whole expression.

We have shown that $a_n(\varrho) = \hat{a}_n(\varrho) + \mathcal{O}\left(\varrho^2\right)$ for $n = 1, 2$. Having assumed $a_n(\varrho) = \hat{a}_n(\varrho) + \mathcal{O}\left(\varrho^2\right)$ to be true for all $1 \leq n \leq m-1$ for some fixed $2 \leq m \in \mathbb{N}$, we proved that $a_m(\varrho) = \hat{a}_m(\varrho) + \mathcal{O}\left(\varrho^2\right)$. We did this via the definitions of d and $\hat{d}$ from a and $\hat{a}$ (respectively), showing that the (equivalent) statement $d_m = \hat{d}_m + \mathcal{O}(\varrho^2)$ holds for each power of κ. Hence by the principle of mathematical induction we have proven our claim, namely

that the recursion for $a_n(\varrho)$ given by (3.7) is solved by

$$\hat{a}_n(\varrho) = 2^n \kappa^n n! \frac{\left(\varrho + \frac{1}{2}\right)_n}{(\varrho+1)_n^2} \sum_{k=0}^{\lfloor \frac{n}{2} \rfloor} \frac{\left(\varrho + \frac{1}{2}\right)_{n-k}}{(n-2k)!k!} \kappa^{-2k}$$

to leading order in ϱ. □

With Lemma 3.3 it is now straightforward to calculate an explicit formula for the coefficients b_n using $b_n = a_n'(0) = \hat{a}_n'(0)$.

Theorem 3.3. *The recursion relation for b_n is solved by*

$$b_n = \frac{1}{4^n} \binom{2n}{n} \sum_{k=0}^{\lfloor \frac{n}{2} \rfloor} \binom{2n-2k}{k, n-k, n-2k} f_{n,k} \left(\frac{\kappa}{2}\right)^{n-2k}$$

with

$$f_{n,k} := 2\mathrm{O}_n + 2\mathrm{O}_{n-k} - 2\mathrm{H}_n,$$

where H_n is the Harmonic number and O_n its odd cousin defined by

$$\mathrm{H}_n := \sum_{k=1}^{n} \frac{1}{k}, \qquad \mathrm{O}_n := \sum_{k=1}^{n} \frac{1}{2k-1}\,.$$

Proof. Using Lemma 3.3 we can simply differentiate $\hat{a}_n(\varrho)$ with respect to ϱ and evaluate at $\varrho = 0$ in order to get b_n. The derivative of the Pochhammer function with respect to its main argument is given by

$$\frac{\partial (x)_n}{\partial x} = (x)_n \left(\psi(a+n) - \psi(a)\right)$$

where the *digamma function*

$$\psi(z) := \frac{\Gamma'(z)}{\Gamma(z)}$$

is the logarithmic derivative of the *Gamma function*, defined for $z \in \mathbb{C}$. Using the digamma function, one can extend Harmonic number to complex

arguments via the definition

$$\mathrm{H}_z := \psi(z+1) + \gamma,$$

where γ is the Euler-Mascheroni constant. Thus in particular we can define the Harmonic number for both integer and half-integer arguments. Using the recursion $\mathrm{H}_n = \mathrm{H}_{n-1} + \frac{1}{n}$ and the fact that $\mathrm{H}_{\frac{1}{2}} := \psi\left(\frac{3}{2}\right) + \gamma = 2 - 2\ln 2$, we arrive at the identity $\mathrm{H}_{n-\frac{1}{2}} = 2\mathrm{O}_n + \mathrm{H}_{-\frac{1}{2}}$. Denote by $\hat{a}_n^k(\varrho)$ the coefficient of κ^{n-2k} in $\hat{a}_n(\varrho)$. The logarithmic derivative of $\hat{a}_n^k(\varrho)$ at $\varrho = 0$ is

$$\frac{a_n^{k\prime}(0)}{a_n^k(0)} = \frac{\hat{a}_n^{k\prime}(0)}{\hat{a}_n^k(0)} = \mathrm{H}_{n-\frac{1}{2}} + \mathrm{H}_{n-k-\frac{1}{2}} - 2\mathrm{H}_n + 4\ln 2 = 2\mathrm{O}_n + 2\mathrm{O}_{n-k} - 2\mathrm{H}_n,$$

and determines the "correction factor" for the coefficient of κ^{2n-k} in b_n. □

To obtain the solutions $I_r(h)$ and $I_s(h)$ of the Picard-Fuchs equation we integrate $T_r(h)$ and $T_s(h)$ term-by-term respectively, and get

$$\begin{aligned} I_r(h) &:= \frac{1}{2\pi}\int T_r(h)\,\mathrm{d}h \\ &= \frac{1}{2\pi}\sum_{n=0}^{\infty}\frac{a_n}{n+1}h^{n+1} \qquad (3.12a) \\ I_s(h) &:= \frac{1}{2\pi}\int T_s(h)\,\mathrm{d}h \\ &= I_r(h)\ln|h| + \frac{1}{2\pi}\sum_{n=0}^{\infty}\frac{1}{n+1}\left\{b_n - \frac{a_n}{n+1}\right\}h^{n+1} \qquad (3.12b) \end{aligned}$$

where the integration constants are fixed by the requirements that $I_r(0) = 0$ and $I_s(h) \to 0$ as $h \to 0$.

3.4 Particular action integrals

Since (3.4) is a linear third order equation, there must be three linearly independent solutions. They are the regular, singular, and constant solutions.

Thus the general solution is an arbitrary linear combination of these, namely

$$I(h) = k_1 I_r(h) + k_2 I_s(h) + k_3, \tag{3.13}$$

and upon differentiating,

$$T(h) = k_1 T_r(h) + k_2 T_s(h).$$

We seek to find the k_i that give the particular solutions corresponding to the closed loops integrals along the paths $\beta_\pm$ as specified in Figure 3.2. The expansions obtained are normalised such that $T_r = 1 + \mathcal{O}(h)$, $2\pi I_r = h + \mathcal{O}(h^2)$, $T_s = \ln|h| + \mathcal{O}(h)$, $2\pi I_s = h\ln|h| + \mathcal{O}(h)$, and so the leading terms are $2\pi I(h) = 2\pi k_3 + k_2 h\ln|h| + k_1 h + \mathcal{O}(h^2)$ and $T(h) = k_1 + k_2\ln|h| + \mathcal{O}(h)$. Thus the constant k_3 is given by $I(0)$, while both k_1 and k_2 are determined by the leading order logarithmically diverging term and the constant term of $T(h)$ for small h.

The particular solutions to be found are given by the integrals $I_{\beta_\pm}$ and $T_{\beta_\pm}$. In order to find the correct linear combinations we need to evaluate these integrals in the limit $h \to 0$. The β integrals at $h = 0$ are computed as real integrals. As mentioned earlier on page 36, when doing this we must halve the complex contour integrals as we convert them into real integrals, as integrating along the branch cuts contributes twice. $I_{\beta_\pm}(0)$ is an elementary and finite real integral that gives

$$\begin{aligned} I_{\beta_\pm}(0) &= \frac{1}{4\pi}\oint_{\beta_\pm} \frac{\mathrm{d}z}{\sqrt{1-\kappa z - z^2}} \\ &= \frac{1}{2\pi}\int_{\Pi[\beta_\pm]} \frac{\mathrm{d}x}{\sqrt{1-\kappa x - x^2}} = \frac{1}{\pi}\tan^{-1}\left(\rho^{\mp 1}\right) . \end{aligned}$$

For the singular integral $T_{\beta_\pm}(h)$, the asymptotic behaviour for small h is

$$\begin{aligned} T_{\beta_\pm}(h) &= \oint_{\beta_\pm} \frac{\mathrm{d}z}{2w(z)\sqrt{2h-z}} = \int_{\Pi[\beta_\pm]} \frac{1}{\sqrt{x(x-2h)}}\frac{1}{\sqrt{1-\kappa x - x^2}}\,\mathrm{d}x \\ &= \pm\ln(\pm h) \mp \frac{1}{2}\ln\left(\frac{64}{\kappa^2+4}\right) + \mathcal{O}(h). \end{aligned}$$

This can be found by defining

$$\varphi(x) := \left[1 - \kappa x - x^2\right]^{-\frac{1}{2}} = \left[(x+\rho)(\rho^{-1} - x)\right]^{-\frac{1}{2}} \in \mathbb{R} \,\forall\, x \in \Pi\,[\beta_\pm]$$

and splitting up the integrals as

$$T_{\beta_\pm}(h) = \int_{\Pi[\beta_\pm]} \frac{\varphi(x) - \varphi(0)}{\sqrt{x(x-2h)}}\,\mathrm{d}x + \int_{\Pi[\beta_\pm]} \frac{\varphi(0)}{\sqrt{x(x-2h)}}\,\mathrm{d}x.$$

The first integral is a convergent elliptic integral, and when $h = 0$ it becomes elementary. For β_+ it gives $-\ln\left(\frac{4\rho^2}{\rho^2+1}\right)$, and for β_- it gives $\ln\left(\frac{4}{\rho^2+1}\right)$. The second integral is divergent when $h \to 0$ but elementary and can be integrated using hyperbolic trigonometric substitutions. For β_+ it gives $-\ln\left(\frac{2}{\rho}\right) + \ln h + \mathcal{O}(h)$, and for β_- it gives $\ln(2\rho) - \ln(-h) + \mathcal{O}(h)$. Adding the two integrals gives the stated result.

From these four integrals the coefficients k_i can be determined as described above and the result is

$$I_{\beta_\pm} = \mp\frac{1}{2}\ln\left(\frac{64}{\kappa^2+4}\right) I_r \pm I_s + \frac{1}{\pi}\tan^{-1}\left(\rho^{\mp 1}\right). \tag{3.14}$$

Remark 3.4. The actions corresponding to approaching the separatrix from either side are related to the residue at infinity of $I(h)$ via

$$2\pi\left(I_{\beta_+}(0) + I_{\beta_-}(0)\right) = \frac{1}{2}\cdot 2\pi\mathrm{i}\operatorname*{Res}_{\infty}\zeta = \pi.$$

This is due to the fact that the total area of the symmetry reduced scaled phase space is π. As mentioned earlier the actual area (without discrete symmetry reduction) enclosed by a single connected contour of $\tilde{\mathsf{H}}$ is twice as large, and each connected component appears twice. Undoing the scaling and discrete symmetry reduction then gives $4\pi\ell^2$, which is the area of the sphere $\mathcal{C}_\ell$ and the complete phase space of the Euler top.

Chapter 4

The symplectic invariants

Equipped with the Frobenius series expansions of the action integrals obtained from the Picard-Fuchs ODE, we can now calculate the semi-global symplectic invariants of the Euler top.

4.1 Revisiting the Birkhoff normal form

The Birkhoff normal form is a series for $h(J)$. From (3.12a) we have

$$2\pi I_r(h) = h + \frac{\kappa}{4}h^2 + \frac{1}{16}\left(3\kappa^2 + 4\right)h^3 + \dots$$

We now aim to calculate I_α via *residue series*. Firstly, we calculate the series expansion of $\zeta(h)$ about $h = 0$, yielding

$$\zeta(h) = \frac{\sqrt{-z}}{w(z)}\left(1 - \frac{h}{z} - \frac{h^2}{2z^2} - \frac{h^3}{2z^3} - \dots\right)\mathrm{d}z.$$

Calculating the action integral I_α involves integrating the differential ζ around the contour α, enclosing the singularity $z = 0$. Thus, we have the residue series

$$\oint_\alpha \zeta(h) = 2\pi\mathrm{i}\operatorname*{Res}_0 \zeta = 2\pi\mathrm{i}\operatorname*{Res}_{z=0}\left\{\frac{\sqrt{-z}}{w(z)}\left(1 - \frac{h}{z} - \frac{h^2}{2z^2} - \frac{h^3}{2z^3} - \dots\right)\right\}.$$

Finally, upon scaling the integral and calculation of each of the residues in the series term-by-term, we arrive at the definition of the real α-cycle action integral, namely

$$I_\alpha(h) := \frac{\mathrm{i}}{2\pi}\oint_\alpha \zeta(h) = h + \frac{\kappa}{4}h^2 + \frac{1}{16}\left(3\kappa^2+4\right)h^3 + \dots \tag{4.1}$$

where we have omitted the subscript $\pm$ for α since the two cases yield the same series expansion. This also shows us that the α-integrals are given explicitly by the regular solution of the Picard-Fuchs ODE, namely

$$I_\alpha = 2\pi I_r,$$

with coefficients given by (3.9). Thus by inverting this series we recover the Birkhoff normal form, so that we can identify $I_\alpha = J$. The fact that the Birkhoff normal form at a hyperbolic point is given by the integral of the α-cycles is a general phenomenon (see [9] for a general proof).

Remark 4.1. One may ponder if a closed formula leading to the coefficients in (4.1) is possible using the residue series. Whilst it is certainly fairly straight forward to obtain a closed formula for the general term in the series of ζ from the Taylor expansion of the square root function, we cannot readily obtain a closed formula for the residue of the general series term. In any case, for the sole purpose of defining the α-cycle action integral, it is much more constructive to calculate the residues term-by-term so as to easily view the connection between I_α and I_r by comparing coefficients.

4.2 The semi-global symplectic invariant

The semi-global symplectic invariant $\sigma(J)$ is the power series given by the regular part of the composition of the action integral with the inverse of the non-singular integral. More precisely there are two cases for $\pm h > 0$, namely

$$2\pi\left(I_{\beta_\pm}\circ I_\alpha^{-1}\right)(J) = \mathcal{A}_\pm \pm J\ln(\pm J) \mp J \mp \sigma(J). \tag{4.2}$$

Here $\mathcal{A}_\pm$ is the area enclosed by the separatrix after discrete symmetry reduction, $\mathcal{A}_\pm = 2\pi I_{\beta_\pm}(0) = 2\tan^{-1}(\rho^{\mp 1})$ so that $\mathcal{A}_+ + \mathcal{A}_- = \pi$. The symplectic invariant σ is hence described in the following Theorem.

Theorem 4.1. *The semi-global symplectic invariant up to order 4 of the Euler top with distinct moments of inertia reduced by discrete symmetry near the unstable equilibrium at its separatrix is given by*

$$\sigma_E(J) = \frac{1}{2}\ln\left(\frac{64}{\kappa^2+4}\right)J - \frac{3\kappa}{8}J^2 - \frac{15\kappa^2+32}{96}J^3 - \frac{5\kappa\,(11\kappa^2+36)}{512}J^4 + \mathcal{O}\left(J^5\right)$$

Proof. The action I_β is given as the series expansions (3.14) and (3.12), whose coefficients were obtained from the Frobenius solution of the Picard-Fuchs equation. The action I_α is similarly given by (4.1), and the inverse of this series is the Birkhoff normal form H^*. Composing I_β with H^* gives the series of the action I_β in terms of the normal form action J, from which the symplectic invariant σ_E can be read off using the definition in (4.2). □

Remark 4.2. Notice that for $\kappa = 0$ ($\Leftrightarrow \rho = 1 \Leftrightarrow \frac{\Theta_3-\Theta_2}{\Theta_2-\Theta_1} = \frac{\Theta_3}{\Theta_1}$) the invariant is an even function of h, so that both sides of the separatrix (for positive and negative h or J) give the same invariant. The linear term has a maximal value of $\ln 4$ at $\kappa = 0$. For positive κ all higher order terms are negative.

More terms of the symplectic invariant up to order 10 are provided in Appendix A.2. The series expansion of σ_E has been numerically verified and agrees well with the values obtained from a direct numerical computation of $I_{\beta_\pm} \circ I_\alpha^{-1}$ as illustrated in Figure 4.1. Even with only ten terms in the series, the discrepancy is well below 10^{-6} for values of h close to 0. In the plot we have displayed 33 data points for $h \in \left(0, \frac{1}{2}\rho^{-1}\right)$ and see divergence when $2h = \rho^{-1}$, as expected.

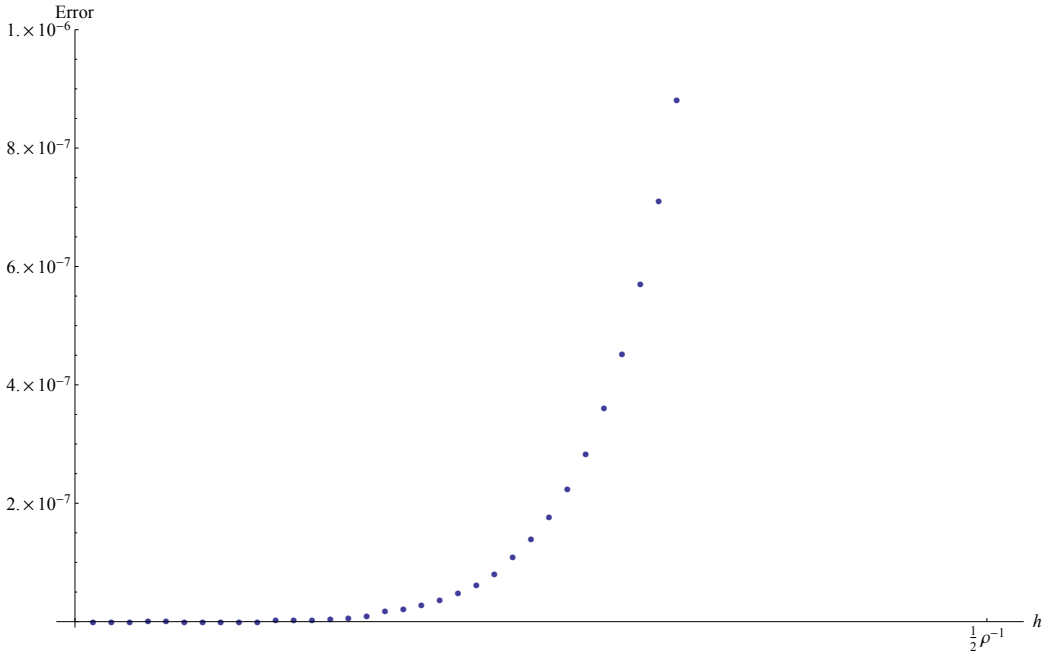

Figure 4.1: The absolute error between calculating the symplectic invariant using the series and using the integrals with $\kappa = 0.5$.

Chapter 5

Convergence of the series

For T and I we now compute the radius of convergence of the expansion found. This can be done analytically. The series for the Birkhoff normal form and the symplectic invariant are then analysed numerically. To analyse the asymptotics of a_n define the ratio

$$r_n := \frac{2n+1}{2n-1}\frac{a_n}{a_{n-1}}$$

and the recursion becomes

$$r_n = \left(4 - \frac{1}{n^2}\right)\left(\frac{\kappa}{2} + \frac{1}{r_{n-1}}\right) \sim 2\kappa + \frac{4}{r_{n-1}}$$

for large n. The leading order iteration has two fixed points at $r = -2\rho^{-1}$ and $r = 2\rho$. The positive fixed point $r = 2\rho$ is stable for $\kappa > 0 \Leftrightarrow \rho > 1$, whilst the negative fixed point $r = -2\rho^{-1}$ is stable for $\kappa < 0 \Leftrightarrow \rho < 1$. The radius of convergence in h is given by

$$R(\rho) := |r_\infty|^{-1} = \tfrac{1}{2}\min(\rho, \rho^{-1}),\ \rho \neq 1$$

and is thus controlled by the roots of w^2 closest to zero (for a discussion of why the $\rho = 1$ case is excluded, see Remark 5.1). For b_n a similar argument works after explicitly controlling the size of $\frac{a_{n-1}}{b_{n-1}}$ and $\frac{a_{n-2}}{b_{n-1}}$, so both series with coefficients a_n and b_n have the same radius of convergence.

The Birkhoff normal form is given by the inverse of the series with coefficients $\frac{a_n}{n+1}$ which converges; we also expect that this series converges due to the theorem of Zung. However, since inverting a series is a highly non-linear process explicit formulas cannot easily be obtained. Similarly, the symplectic in variant is based on the convergent series with coefficients $\frac{b_n}{n+1} - \frac{a_n}{(n+1)^2}$ together with the Birkhoff normal form, so again we expect convergence.

We investigate the radius of convergence (using the ratio formula) of both the Birkhoff normal form and the symplectic invariant numerically, as illustrated in Figure 5.1. In calculating the ratios of coefficients of successive powers of J, we obtain the radii of convergence. Figure 5.1 shows us that these converge to a non-zero value, and thus the radii of convergence of both the Birkhoff normal form and the symplectic invariant appears to be non-zero. In Figure 5.1a we fixed $\kappa = 10$ and varied N (as defined in the figure). The dashed red horizontal line is the radius of convergence of a_n, b_n which is given by $R \approx 0.0495098$ for this value of κ. The curve passing through the 40 discrete data points (chopping off the first 10 due to their irregular behaviour) was implemented in Mathematica using the FindFit least squares algorithm. We found that the decaying exponential $0.0648161 + 0.018825e^{-0.230762N^{0.677788}}$ fitted the data well, yielding a horizontal asymptote larger than the value of R. In Figure 5.1b we fixed $N = 14, 15$ in the ratio formula given in Figure 5.1a and varied κ instead, yielding the dark dashed blue and light dotted red curves respectively. The thick black curve plots R as a function of κ. The two non-solid coloured curves are coarse approximations (due to computational limitations) of the radius of convergence. The results for the Birkhoff normal form and the symplectic invariant are the same as the data points overlap and curves coincide for both. For various values of κ we found that the ratios of successive coefficients tend to non-zero constants. We found that the data does not share the same radius of convergence, rather the radius of convergence is actually larger; this is evident in both plots. In Figure 5.1a the fitted curve decreases very slowly and is too large in comparison to the dashed red line to converge to it. In Figure 5.1b we see that both

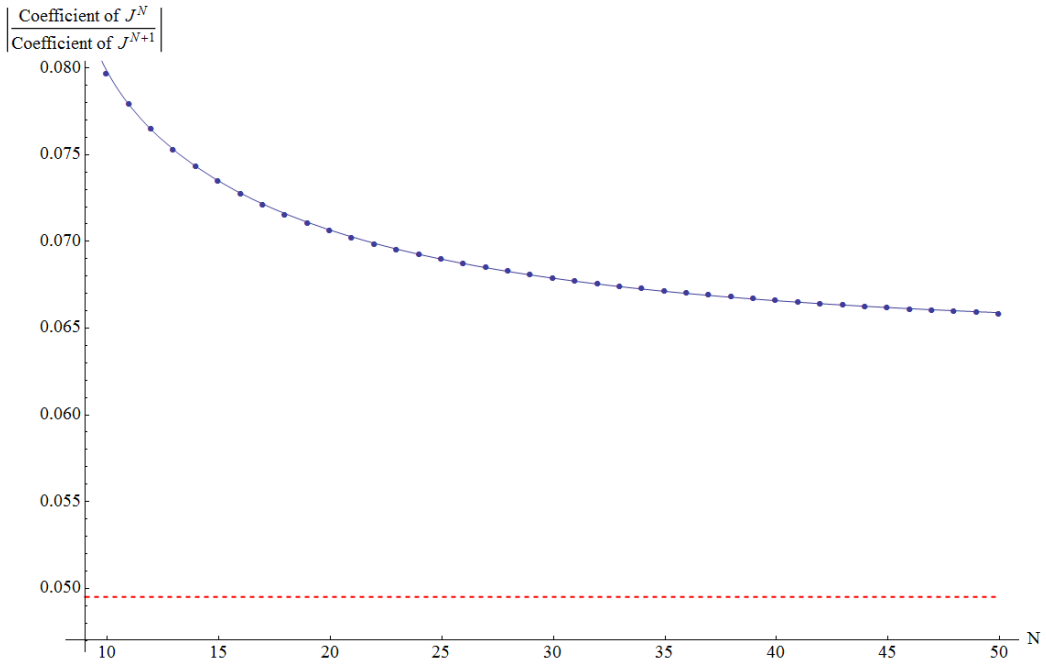

(a) Ratios tending to the radius of convergence

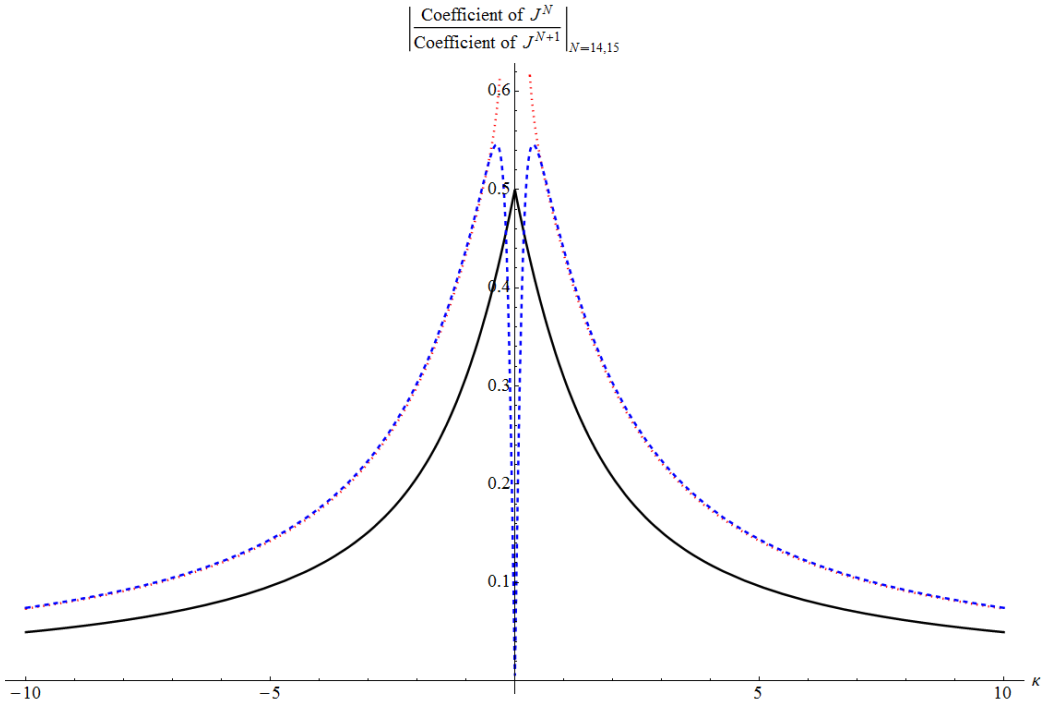

(b) Radius of convergence as a function of κ

Figure 5.1: Numerical analysis of the radius of convergence of the Birkhoff normal form and symplectic invariant.

dashed coloured curves are significantly larger than the solid black curve for all values of κ; by observing the morphology of these curves as N increases (which can be done numerically using Mathematica), we conclude that it is highly unlikely that the two dashed coloured curves will converge to the solid black curve. Thus the ratios must converge to a significantly larger value than R by at least 25%.

Remark 5.1. Clearly Figure 5.1b shows that R breaks down at $\kappa = 0 \Leftrightarrow \rho = 1$. This is because in this case all the *even* powers of J get killed off and we have

$$\begin{aligned} H^*(J) &= J - \frac{1}{4}J^3 + \mathcal{O}\left(J^5\right) \\ \sigma_E(J) &= 2\ln 2\, J - \frac{32}{96}J^3 + \mathcal{O}\left(J^5\right) \end{aligned}$$

for the Birkhoff normal form and symplectic invariant. Similarly we find that the coefficients a_n and b_n vanish whenever n is *odd*; the coefficients are $1, 0, \frac{3}{4}, 0, \frac{105}{64}, 0, \ldots$ and $0, 0, \frac{5}{4}, 0, \frac{389}{128}, 0 \ldots$ respectively.

Because of this, naïvely using the traditional ratio formula for the radius of convergence causes $R(1)$ to oscillate between 0 and ∞ for even and odd values of n respectively, rendering the ratio formula for the radius of convergence undefined in the $\rho = 1$ case. To alleviate this problem, one must compute *every second* term. For example, we define the radius of convergence of a_n in this scenario to be

$$R_0 := \lim_{n\to\infty} \left|\frac{a_{n-2}}{a_n}\right|_{\rho=1}$$

and we compute it from equation (3.8). Observe that

$$\begin{aligned} \frac{a_n}{a_{n-2}} &= \frac{\kappa}{2}\frac{(2n-1)^2}{n^2}\frac{a_{n-1}}{a_{n-2}} + \frac{(2n-1)(2n-3)}{n^2} \\ &\sim \frac{2\kappa}{R(\rho)} + 4 \quad \text{for large } n. \end{aligned}$$

We can now take the limit as $\kappa \to 0 \Leftrightarrow \rho \to 1$, since these parameters can

take all values in $\mathbb{R}$ and $(0, \infty)$ respectively. Observing that $\lim_{\rho \to 1} R(\rho) = \frac{1}{2}$ is bounded in this limit, we find that $R_0 = \frac{1}{4}$ in the above equation. We similarly find that b_n has the same radius of convergence in the $\rho = 1 \Leftrightarrow \kappa = 0$ case, using the same arguments mentioned earlier on page 54.

Having established that the coefficients a_n and b_n converge within a non-zero radius of convergence, we can argue in a similar fashion to before that the Birkhoff normal form and thus also the symplectic invariant converge within a non-zero radius of convergence. Numerically we find that both series have a radius of convergence greater than approximately 0.32 (to two decimal places) when setting $\kappa = 0$ in the coefficients.

Chapter 6

Conclusion

The main result of this work was to explicitly calculate the semi-global symplectic invariants of the Euler top near the hyperbolic equilibria. There are two motivations for calculating these invariants, and they will be presented in this conclusion. One is to obtain a means to compare the Euler top to other systems, and in particular, we will compare the Euler top to the pendulum. In the past, other notions of equivalence have been used to study the Euler top in [3, 4, 5, 24]. Equipped with the semi-global symplectic invariant of the Euler top, we can now check equivalence with other dynamical systems. Another motivation is the connection between the symplectic invariants and the tumbling phenomenon of the unstable axis rotation. We will discuss where further work may lead, and why this is interesting and of relevance to real-world applications.

6.1 Non-equivalence with the pendulum

Attempts have been made to find notions of equivalence between the Euler top and the pendulum. A notable theorem is given in [15], whereby Holm and Marsden prove that rigid-body motion reduces down to pendulum motion on the contour lines. However, these systems are *linked*, not *equivalent* in the sense that we are interested in. The Euler top is a bi-Hamiltonian system, meaning that it can be written using a different Poisson structure. But only

the Poisson structure $\hat{L}$ comes from the original physical system.

Before we proceed, we need to check that the topologies of the separatrices near the hyperbolic equilibrium point of the Euler top and the pendulum are the same, as is required by Theorem 1.3. Initially they are not (two joined circles intersecting twice versus a "figure-eight" respectively), however after discrete symmetry reduction they are the same. Then we may proceed to show that the two systems are not equivalent in the sense of Theorem 1.3. The semi-global symplectic invariant (at the unstable hyperbolic equilibrium) of the pendulum is given in [9] to leading order as

$$\sigma_P(J) = \ln 32\, J + \mathcal{O}\left(J^2\right).$$

For the pendulum to be equivalent to a particular Euler top, we would need to be able to set

$$\sigma_E(J) = \frac{1}{2} \ln\left(\frac{64}{\kappa^2 + 4}\right) J + \mathcal{O}\left(J^2\right)$$

to be equivalent to σ_P. We first try to set them equivalent to leading order. This would require setting $\kappa = \pm\frac{3}{4}\mathrm{i}\sqrt{7}$, which is impossible since we require $\kappa \in \mathbb{R}$. Since there is no valid κ that maps the leading order coefficient of the symplectic invariant of the Euler top to the leading order coefficient of the symplectic invariant of the pendulum, we conclude that there is no such special Euler top that is equivalent to the pendulum.

6.2 Physical connections and further research

The "tumbling" of the book as described in Figure 1.1 is an interesting phenomenon. Understanding the exact nature of this unstable motion would be of great application and importance to the physical world. We believe that the tumbling motion is encoded within the symplectic invariants. Future work in this area may reveal exactly how these Taylor coefficients dictate how the book tumbles in such an intricate way when rotated about its unstable axis. Physicists are interested in the rotations of more important objects

other than books, and there would be countless applications to rigid bodies in the real world, from sports right through to aerospace. Further research in this area would also include comparing semi-global symplectic invariants of other dynamical systems, to either prove or disprove equivalence. Such comparisons will no doubt help us understand more about each individual system, as well as any underlying similarities or differences between them.

Bibliography

[1] V. I. Arnold. *Mathematical Methods of Classical Mechanics (Graduate Texts in Mathematics)*. Springer, 2nd edition, May 1989.

[2] G.D. Birkhoff. *Dynamical systems*, volume 9. American Mathematical Society, 1927.

[3] A. V. Bolsinov and H. R. Dullin. On the Euler case in rigid body dynamics and the Jacobi problem (in Russian). *Regular and Chaotic Dynamics*, 2:13–25, 1997.

[4] A. V. Bolsinov and A. T. Fomenko. The geodesic flow of an ellipsoid is orbitally equivalent to the integrable Euler case in the dynamics of a rigid body. *Doklady Akademii Nauk*, 339(3):253–296, 1994.

[5] A.V. Bolsinov and A.T. Fomenko. *Integrable Hamiltonian systems: geometry, topology, classification*. Chapman & Hall/CRC, 2004.

[6] W.E. Boyce and R.C. DiPrima. *Elementary differential equations and boundary value problems*. Wiley, 2001.

[7] C.H. Clemens. *A scrapbook of complex curve theory*. University series in mathematics. Plenum Press, 1980.

[8] J. Dufour, P. Molino, and A. Toulet. Classification des systèmes intégrables en dimension 2 et invariants des modèles de Fomenko. *Comptes Rendus. Mathématique. Académie des Sciences, Paris*, 318(10):949–952, 1994.

[9] H.R. Dullin. Semi-global symplectic invariants of the spherical pendulum. *arXiv e-prints*, arXiv:1108.4962, August 2011.

[10] H.R. Dullin and S. V. Ngoc. Symplectic invariants near hyperbolic-hyperbolic points. *Regular and Chaotic Dynamics*, 12:689–716, 2007.

[11] H.R. Dullin, P. H. Richter, A. P. Veselov, and H. Waalkens. Actions of the Neumann systems via Picard-Fuchs equations. *Physica D: Nonlinear Phenomena*, 155(155):159–183, 2001.

[12] L. Euler. Decouverte d'un nouveau principe de mecanique. *Mémoires de l'académie des sciences de Berlin*, 6:185–217, 1752.

[13] L. Euler. Du mouvement de rotation des corps solides autour d'un axe variable. *Mémoires de l'académie des sciences de Berlin*, 14:154–193, 1765.

[14] F. Fassò. The Euler-Poinsot top: A non-commutatively integrable system without global action-angle coordinates. *Zeitschrift für Angewandte Mathematik und Physik*, 47(6):953–976, 1996.

[15] D.D. Holm and J.E. Marsden. The rotor and the pendulum. *Symplectic geometry and mathematical physics,(Progress in Mathematics), Birkh auser, Boston*, 99:189–203, 1991. P. Donato et al., eds.

[16] D.D. Holm, T. Schmah, C. Stoica, and D.C.P. Ellis. *Geometric Mechanics and Symmetry: From Finite to Infinite Dimensions*. Oxford University Press, 2009.

[17] L. D. Landau and E. M. Lifshitz. *Mechanics, Third Edition: Volume 1 (Course of Theoretical Physics)*. Butterworth-Heinemann, 3 edition, January 1976.

[18] E. Leimanis. *The General Problem of the Motion of Coupled Rigid Bodies about a Fixed Point*. Springer, 1965.

[19] J. E. Marsden and T. S. Ratiu. *Introduction to Mechanics and Symmetry*. Springer, New York, 1994.

[20] K. Meyer, G. Hall, and D. Offin. *Introduction to Hamiltonian Dynamical Systems and the N-Body Problem.* Applied Mathematical Sciences. Springer, 2010.

[21] Richard Montgomery. Gauge theory of the falling cat. *Fields Inst. Commun*, 1:193–218, 1993.

[22] J. Moser. The analytic invariants of an area-preserving mapping near a hyperbolic fixed point. *Communications on Pure and Applied Mathematics*, 9(4):673–692, 1956.

[23] S. V. Ngoc. On semi-global invariants for focus-focus singularities. *Topology*, 42(2):365–380, 2003.

[24] O. E. Orël. On the nonconjugacy of the Euler case in the dynamics of a rigid body and on the Jacobi problem of geodesics on an ellipsoid. *Matematicheskie Zametki*, 61(2):252–258, 1997.

[25] G. Papadopoulos and H.R. Dullin. Semi-global symplectic invariants of the Euler top. *arXiv e-prints*, arXiv:1210.6522, 2012.

[26] A. Pelayo and S. V. Ngoc. Hamiltonian dynamics and spectral theory for spin-oscillators. *Communications in Mathematical Physics*, 309:123–154, 2012.

[27] R. Talman. *Geometric mechanics.* Wiley-VCH, 2008.

[28] A. Toulet. *Classification of integrable systems on two-dimensional symplectic manifolds.* PhD thesis, Montpellier II University, September 1996.

[29] W. Walter and R. Thompson. *Ordinary Differential Equations.* Springer, 1998.

[30] Nguyen Tien Zung. Convergence versus integrability in birkhoff normal form. *Annals of mathematics*, pages 141–156, 2005.

Appendix A

Calculation of higher order terms

A.1 Birkhoff normal form

N	Coefficient of J^N
5	$-\frac{3\left(\kappa^2+4\right)\left(11\kappa^2+12\right)}{1024}$
6	$-\frac{7\kappa\left(\kappa^2+4\right)\left(9\kappa^2+20\right)}{2048}$
7	$-\frac{\left(\kappa^2+4\right)\left(527\kappa^4+1776\kappa^2+720\right)}{16384}$
8	$-\frac{9\kappa\left(\kappa^2+4\right)\left(1043\kappa^4+4720\kappa^2+4240\right)}{262144}$
9	$-\frac{5\left(\kappa^2+4\right)\left(35009\kappa^6+199020\kappa^4+283952\kappa^2+60992\right)}{4194304}$
10	$-\frac{11\kappa\left(\kappa^2+4\right)\left(38415\kappa^6+263012\kappa^4+518992\kappa^2+260800\right)}{8388608}$

A.2 Symplectic invariant

N	Coefficient of J^N
5	$-\frac{945\kappa^4+4200\kappa^2+2672}{10240}$
6	$-\frac{7\kappa\left(527\kappa^4+2960\kappa^2+3600\right)}{40960}$
7	$-\frac{65709\kappa^6+446040\kappa^4+801360\kappa^2+241664}{688128}$
8	$-\frac{15\kappa\left(105027\kappa^6+835884\kappa^4+1987664\kappa^2+1280832\right)}{14680064}$
9	$-\frac{19015425\kappa^8+173587920\kappa^6+513802080\kappa^4+516384000\kappa^2+90566912}{150994944}$
10	$-\frac{11\kappa\left(6991255\kappa^8+71998560\kappa^6+255042144\kappa^4+350638080\kappa^2+140532480\right)}{503316480}$

Appendix B

Analysis of κ

We analyse the behaviour of κ for a range of values. To do this, we plot a variety of contours for κ in a convenient co-ordinate system. First we normalise the moments of inertia such that $\Theta_1 + \Theta_2 + \Theta_3 = 1$. Since the moments of inertia are positive, this yields a plane in the positive octant of $\mathbb{R}^3$, namely, a triangle with vertices $(1,0,0), (0,1,0), (0,0,1)$. The following inequalities to be satisfied are

$$0 < \Theta_1 < \Theta_2 < \Theta_3 \text{ (orderings (1.1))} ,$$

$$\Theta_i < \Theta_j + \Theta_k \text{ (triangle inequalities (1.2))},$$

$$0 < \Theta_i < 1 \text{ (first octant)}.$$

We construct a new right-handed co-ordinate system (X, Y, Z) that has its origin is located at $(\Theta_1, \Theta_2, \Theta_3) = \left(\frac{1}{3}, \frac{1}{3}, \frac{1}{3}\right)$, Z-axis in the direction pointing outward perpendicular to the plane, Y-axis along the line joining the two points $\left(\frac{1}{3}, \frac{1}{3}, \frac{1}{3}\right), (0,0,1)$ and X-axis parallel to the bottom edge of the triangle. The transformation between co-ordinates is given by

$$\begin{pmatrix} X \\ Y \\ Z \end{pmatrix} = \begin{pmatrix} \frac{-1}{\sqrt{2}} & \frac{1}{\sqrt{2}} & 0 \\ \frac{-1}{\sqrt{6}} & \frac{-1}{\sqrt{6}} & \frac{2}{\sqrt{6}} \\ \frac{1}{\sqrt{3}} & \frac{1}{\sqrt{3}} & \frac{1}{\sqrt{3}} \end{pmatrix} \begin{pmatrix} \Theta_1 - \frac{1}{3} \\ \Theta_2 - \frac{1}{3} \\ \Theta_3 - \frac{1}{3} \end{pmatrix}.$$

In these co-ordinates, the triangular plane lies in the XY-plane, that is $Z = 0$, and the inequalities become

$$3\sqrt{2}\,X + \sqrt{6}\,Y < 2 \wedge \sqrt{6}\,Y < 3\sqrt{2}\,X + 2 \wedge \sqrt{6}\,Y + 1 > 0$$

$$2\sqrt{6}\,Y < 1 \wedge \sqrt{6}\,Y + 1 > 3\sqrt{2}\,X \wedge 3\sqrt{2}\,X + \sqrt{6}\,Y + 1 > 0$$

$$X > 0 \wedge \sqrt{3}\,Y > X \wedge 3\sqrt{2}\,X + \sqrt{6}\,Y < 2$$

respectively. The intersection of these three (which is where the contours of κ live) gives

$$X > 0 \wedge 2\sqrt{6}\,Y < 1 \wedge X < \sqrt{3}\,Y. \tag{B.1}$$

We plotted 21 equally-spaced contours with $|\kappa| \leq 5$ in the normalization plane, as displayed in Figure B.1.The dashed black contour corresponds to $\kappa = 0$. Those to the left plotted in light blue and to the right in dark red correspond to positive and negative values of κ respectively. Note that the positive contours tend to $X = 0$ quickly, whilst the negative contours tend to $Y = \frac{1}{\sqrt{3}}X$ slowly. The largest upright centred blue triangle is the original whole normalization plane in the positive octant. The inverted inscribed centred purple triangle is the region which satisfies the triangle inequalities. The tall upright beige triangle in the first quadrant corresponds to the orderings of the moments of inertia. Finally, the smallest green triangle which contains the contours, is the intersection of these three regions.

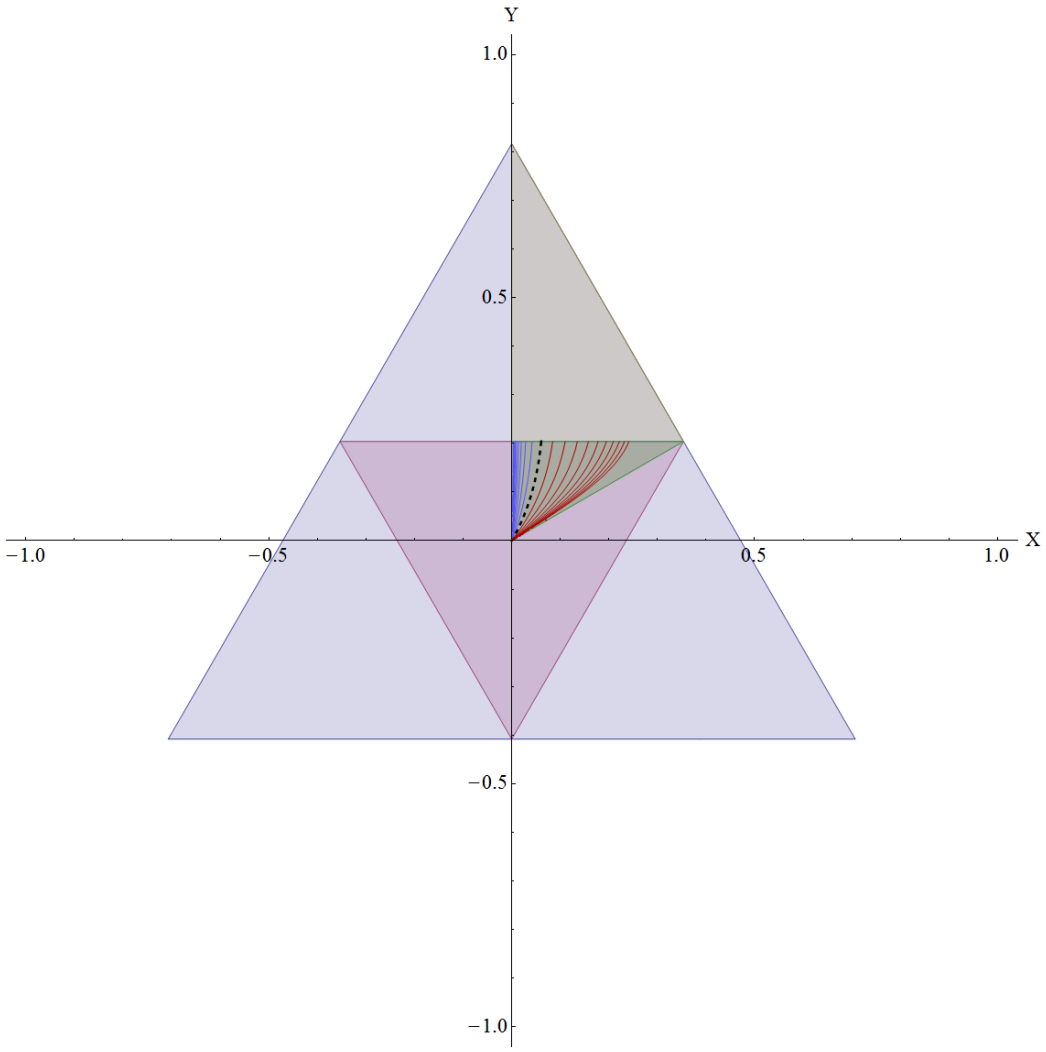

Figure B.1: Contour plot of κ satisfying the inequalities (B.1).

Acknowledgements

First and foremost, I would like to thank my supervisor Holger Dullin for his incredible dedication of time and patience throughout the four year long journey of this research; his contributions to this work cannot be overstated. The examiners, Professors Peter H. Richter and San Vu Ngoc, provided some very gratifying comments as well as constructive criticisms which I used to improve the quality of this final submitted thesis, and I am truly grateful for their contributions. The School of Mathematics and Statistics at the University of Sydney have also shown great support in providing me with, resources, aid and casual employment to fund my expenses during this research. My sincere thanks are also extended to Samuel Müller for proof-reading my thesis and providing valuable feedback at very short notice. Finally, I send my warmest gratitude to my closest friends and family whom have supported me in every way possible; through even the toughest of times, they never failed to believe in my ability to succeed in completing this research.